ANTIOXIDANTS & REDOX SIGNALING
Volume 10, Number 1, 2008

DOI: 10.1089/ars.2007.1705

Comprehensive Invited Review

Molecular Mechanism of Proton Translocation by Cytochrome *c* Oxidase

ILYA BELEVICH and MICHAEL I. VERKHOVSKY

Reviewing Editors: Antonio Barrientos, Enrique Cadenas, Robert Genis, Sergio Papa and Alexei Stuchebrukhov

Helsinki Bioenergetics Group, Program for Structural Biology and Biophysics, Institute of Biotechnology, University of Helsinki, Helsinki, Finland.

ABSTRACT

Cytochrome *c* oxidase (CcO) is a terminal protein of the respiratory chain in eukaryotes and some bacteria. It catalyzes most of the biologic oxygen consumption on earth done by aerobic organisms. During the catalytic reaction, CcO reduces dioxygen to water and uses the energy released in this process to maintain the electrochemical proton gradient by functioning as a redox-linked proton pump. Even though the structures of several terminal oxidases are known, they are not sufficient in themselves to explain the molecular mechanism of proton pumping. Thus, additional extensive studies of CcO by varieties of biophysical and biochemical approaches are involved to shed light on the mechanism of proton translocation. In this review, we summarize the current level of knowledge about CcO, including the latest model developed to explain the CcO proton-pumping mechanism. *Antioxid. Redox Signal.* 10, 1–29.

I. INTRODUCTION

A. Energy cycle in living organisms

All living organisms require energy for growth and reproduction. However, the quantity of primary energy sources on earth is limited, and the most important function of all organisms is to find a means of energy supply. The major source of energy in the biosphere is sunlight. About 3 billion years ago, some bacteria learned to use the energy of photons from the sun and convert it into the energy of chemical bonds in a process called photosynthesis. In this complex process, the energy of a light quantum drives the electron flux from water to carbon dioxide, forming carbohydrates [mainly glucose (Eq. 1), sucrose, and starch], which eventually form the basis for the building of biomass and growth. As a side product of the photosynthetic reaction, molecular oxygen is released into the atmosphere.

$$6\ CO_2 + H_2O \xrightarrow{hv,photosynthesis} C_6H_{12}O_6 + 6\ O_2 \qquad (1)$$

Some time after the formation of the earth, the amount of dioxygen in the atmosphere was greatly increased, and ~2–2.5 billion years ago, a new line of organisms appeared. This new form of life was able to obtain the energy it needed by transferring electrons from foodstuffs, created in photosynthesis, to oxygen, thereby releasing a great deal of energy (Eq. 2). This latter process is called respiration.

$$C_6H_{12}O_6 + 6\ O_2 \xrightarrow{respiration} 6\ CO_2 + 6\ H_2O + energy\ (ATP), \qquad (2)$$

Thus, taken together, these two processes form a closed carbon cycle, responsible for the circulation and transformation of energy among living organisms on earth.

B. Cellular respiration

The catabolic reaction in higher organisms consists of three main stages. The first stage is glycolysis, and it takes place in the cytoplasm of the cell. In this process, glucose and other sugars are transformed into three-carbon molecules of pyruvate, with the generation of ATP and NADH. However, the amount of ATP and NADH formed at this stage is rather small, especially when compared with the further steps of pyruvate disintegration.

The next two steps of energy transformation occur in mitochondria. The mitochondrion consists of two closed membrane layers identified as the outer and inner membranes, which divide the mitochondrion into two isolated compartments: the internal matrix and intermembrane space. The outer membrane, which encloses the entire organelle, has a large number of pores formed by the protein *porin*. Porin contains a relatively large internal channel that makes the outer membrane permeable for all kinds of molecules up to 1,500 Da. In contrast, the inner membrane is impermeable to any water-soluble molecules and ions, and transport of molecules here is done selectively through specific transporters. The main physiologic functions of the inner membrane are to home enzymatic complexes of the respiratory chain (also known as the electron-transport chain) and to maintain an electrochemical transmembrane proton gradient, which is subsequently used for ATP synthesis (140). Depending on environmental conditions, the inner mitochondrial membrane can be extremely enlarged into the matrix space, increasing its capacity to contain the proteins of the respiratory chain. Unlike eukaryotes, prokaryotes lack mitochondria, and in these organisms the enzymes of the respiratory chain are situated in the cytoplasmic membrane.

At the second stage of the catabolic reaction, the molecule of pyruvate is transferred into the matrix compartment of the mitochondria, where it enters the citric acid cycle (*Krebs cycle*), which results in its complete oxidation to carbon dioxide. In this sequential process, the oxidation of one molecule of pyruvate produces one molecule of ATP, one molecule of $FADH_2$, and three molecules of NADH. The latter two substances are used as electron donors in the latest stage of cellular respiration by the enzymes of the respiratory chain.

The respiratory chain (Fig. 1) consists of four membrane-bound protein complexes containing redox-active cofactors (198). The first enzyme in this chain is complex I (NADH:ubiquinone oxidoreductase or NADH dehydrogenase). Complex I is the largest enzyme of the respiratory chain, composed of up to 45 different subunits (52) with noncovalently bound flavin mononucleotide (FMN) and at least eight iron–sulfur clusters (Fe-S) as prosthetic groups (95). Complex I receives electrons from NADH and uses them to reduce the quinone pool in the membrane. This reaction

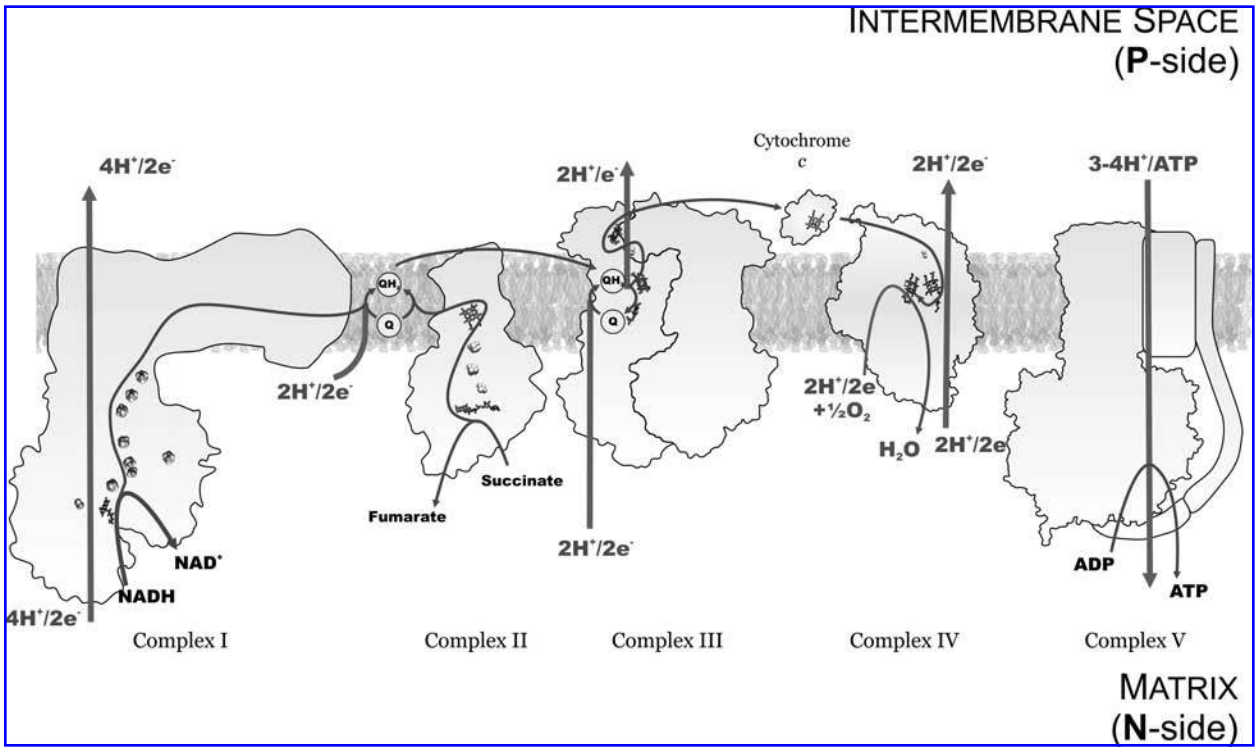

FIG. 1. Schematic representation of the mitochondrial inner membrane, including the enzymes of the respiratory chain and ATP synthase. The electrons originating from the oxidation of NADH and succinate are transferred through complexes I, III, and IV to the ultimate electron acceptor: dioxygen. Translocation of electrons triggers proton movement from the N-side to the P-side of the membrane and formation of the electrochemical proton gradient ($\Delta\mu_H{}^+$). The amplitude of $\Delta\mu_H{}^+$ is maintained at a value of ~200–220 mV and used by ATP synthase (complex V) for formation of ATP.

is coupled to proton translocation across the membrane in the stoichiometry of two protons per electron (35, 97, 248, 264). It should be noted, however, that in some organisms [*e.g.*, the yeast *Saccharomyces cerevisiae* (baker's yeast)], the mitochondrial respiratory chain does not contain complex I as such, but several alternative NADH dehydrogenases. These alternative dehydrogenases can oxidize matrix and cytoplasmic NADH but do not perform proton pumping (109).

The reduced quinone pool is also maintained by complex II (succinate dehydrogenase), which is a component of the citric acid cycle. Complex II contains a covalently bound FAD (flavin-adenine dinucleotide) and several Fe-S clusters as redox cofactors and couples the reaction of succinate oxidation to the reduction of ubiquinone (100). Complex II is not involved in proton translocation across the membrane and serves only as an electron entry point to the energy-transducing part.

Complex III (ubiquinol:cytochrome *c* oxidoreductase or bc_1 complex) has 11 subunits with several redox centers: two protohemes (cytochromes *b*), membrane-anchored cytochrome c_1, and Rieske-type center (Fe_2S_2). Complex III transfers electrons from ubiquinol to cytochrome *c* and translocates one charge across the membrane dielectric for each electron delivered to cytochrome *c* by a mechanism known as the protonmotive Q-cycle (56, 141).

Finally, the terminal oxidase complex IV (cytochrome *c* oxidase, CcO) uses the electrons from cytochrome *c* to reduce dioxygen to water and links this process to proton pumping across the membrane. Mammalian CcO consists of 13 subunits and has four redox-active centers: a bimetallic copper site (Cu_A), two hemes (*a* and a_3, the subscript "3" denoting certain specific chemical and spectroscopic properties of oxygen-binding heme), and another copper atom (Cu_B). Heme a_3 and Cu_B together form a catalytic site where all the chemistry of oxygen reduction to water occurs.

During the respiration process, electrons from NADH are sequentially transferred through all enzymes of the respiratory chain, releasing energy step by step, to the terminal electron acceptor, dioxygen. The idea of this process is to release energy from electron transfer, not all at once, but in small portions to drive proton translocation across the membrane and creation of a transmembrane electrochemical gradient of protons ($\Delta\mu_H{}^+$). The full decrease in energy from NADH to dioxygen is ~1.15 V, and if it were transformed into electric potential in a single step, it would create such a large electric field that the membrane could not sustain it. Thus, the respiratory chain works as a molecular transformer that keeps low voltage on the membrane (~200 mV) but proportionately increases the current. Because the potential on the mitochondrial membrane is in ~5 times smaller than the overall decrease of energy, the transfer of each electron through the respiratory chain results in translocation of five charges (protons) across the membrane.

The created $\Delta\mu_H{}^+$ is mostly used by ATP synthase (complex V) for formation of ATP (140, 213). The sequential oxidation of glucose to carbon dioxide is extremely efficient and provides sufficient energy for formation of up to 31 molecules of ATP per molecule of glucose.

II. FUNCTION OF CYTOCHROME *C* OXIDASE

CcO catalyzes the final step of the respiration: reduction of molecular oxygen. Reduction of one dioxygen to water requires four electrons that are supplied one by one from the water-soluble cytochrome *c* on the P-side, and four protons, taken up from the N-side of the membrane:

$$4\ cyt\ c_P^{2+} + 4\ H_N^+ + O_2 \rightarrow 4\ cyt\ c_P^{3+} + 2\ H_2O + energy$$

Altogether, several main aspects are included in the functioning of CcO. First, even though the reaction of oxygen reduction to water is an exergonic process, coupled to release of large amounts of energy, this reaction does not proceed spontaneously under normal conditions. The reason is the high activation barrier. Hence, the first main role of CcO is to form favorable conditions for catalysis and to facilitate the process of oxygen reduction to water.

Second, the energy released in the reaction of oxygen reduction is conserved in the form of a transmembrane electrochemical gradient of protons across the membrane ($\Delta\mu_H{}^+$). Formation of $\Delta\mu_H{}^+$ by CcO is based on two principles: vectorial chemistry and proton pumping. Because the protons and electrons for oxygen reduction to water are taken from different sides of the membrane, this results in net transfer of four charges across the membrane. At the same time, the enzyme is able not only to catalyze the oxygen reduction but also to use the released energy for proton pumping. In 1977, Wikström (255) showed that reduction of molecular oxygen to water by CcO is linked to pumping of four protons across the membrane dielectric. Hence, the overall reaction done by cytochrome *c* oxidase can be described by the following equation:

$$4\ cyt\ c_P^{2+} + 8\ H_N^+ + O_2 \rightarrow 4\ cyt\ c_P^{3+} + 2\ H_2O + 4\ H_P^+.$$

Third, all processes of oxygen redox chemistry might be extremely dangerous for a cell because of the possible formation in these reactions of highly toxic reactive oxygen species (ROS: hydroxyl radical, hydrogen peroxide, and superoxide). These oxygen compounds can induce chain reactions of oxidative damage of fatty acids and other lipids, DNA molecules, proteins, and so on. Therefore, the mechanism of oxygen catalysis in cytochrome *c* oxidase is organized such that it excludes the formation of ROS (see later) and assures complete reduction of oxygen to water (19).

III. BRANCHING OF THE RESPIRATORY CHAIN IN THE AEROBIC ORGANISMS

In contrast to eukaryotes, in which only one type of terminal oxidase (aa_3-type cytochrome *c* oxidase) is present, the respiratory chains in bacteria can vary extensively (9, 70) and have multiple types of terminal oxidases (Fig. 2). The main function of such branching is to provide bacteria with better adaptability in a variety of environmental growth conditions. In brief,

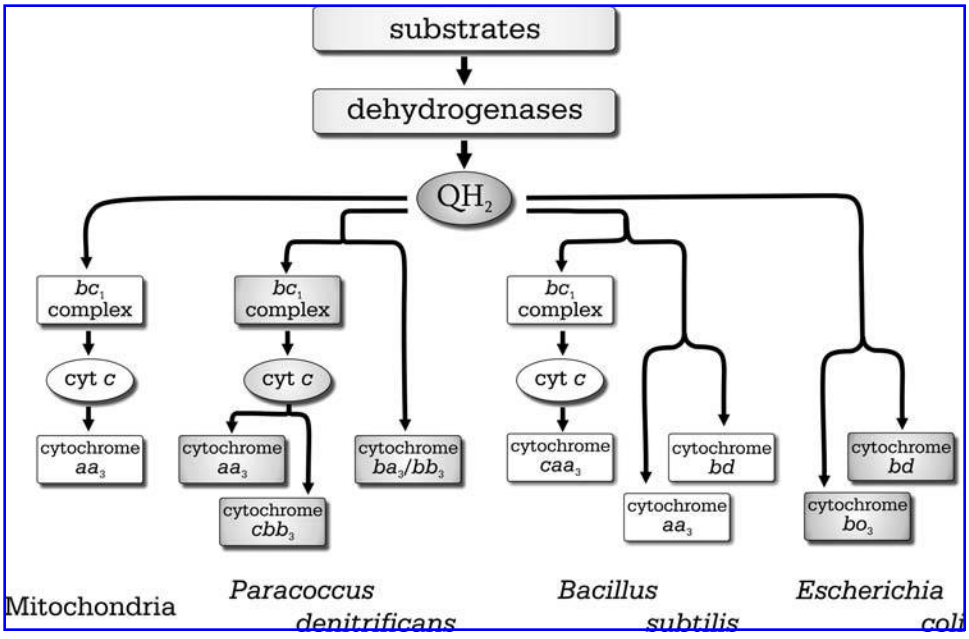

FIG. 2. Several examples of the respiratory chains in bacteria and higher organisms. In contrast to higher organisms, bacteria usually combine several different systems for energy formation and, depending on environmental conditions, may prefer one way to another.

bacteria design the composition of the respiratory pathways for optimal growth based on the following factors:

- *Maintain the highest possible coupling efficiency* (H^+/e^- ratio) in the present environmental conditions for maximal yield of ATP. For example, if the oxygen tension in the growth medium is high, then the terminal oxidases in *Escherichia coli* will be mostly represented by high-efficient cytochrome bo_3, which use the energy of oxygen reduction to water to pump protons. Otherwise, in low-oxygen conditions, the most pronounced will be the expression of cytochrome *bd* (170, 183). This oxidase has a higher affinity to oxygen (24) but does not pump protons (139, 174). Hence, the overall amount of energy formed in low-oxygen conditions will be decreased, but the respiratory chain will still be able to work, providing bacteria with energy.
- *Rapid removal of excess reducing equivalents* such as NADH/NADPH. Even though the main function of the respiratory chain is to generate $\Delta\mu_H{}^+$, it also regulates the NAD^+/NADH ratio by eliminating excess reducing equivalents. This function is very important for organisms that have access to some alternative sources of energy, like photosynthesis. For instance, under high-light conditions in cyanobacteria, the reducing equivalents are formed extremely fast, and both CcO and b_6f complex together cannot prevent overreduction of the quinone pool in the membrane. In such a situation, cytochrome *bd* starts to play an important role because of its lower coupling efficiency (28).
- *Regulation of intracellular oxygen concentration*. Under some specific conditions, it might be very important for bacteria to decrease the intracellular amounts of oxygen to protect oxygen-sensitive enzymes from inhibition. As in nitro-

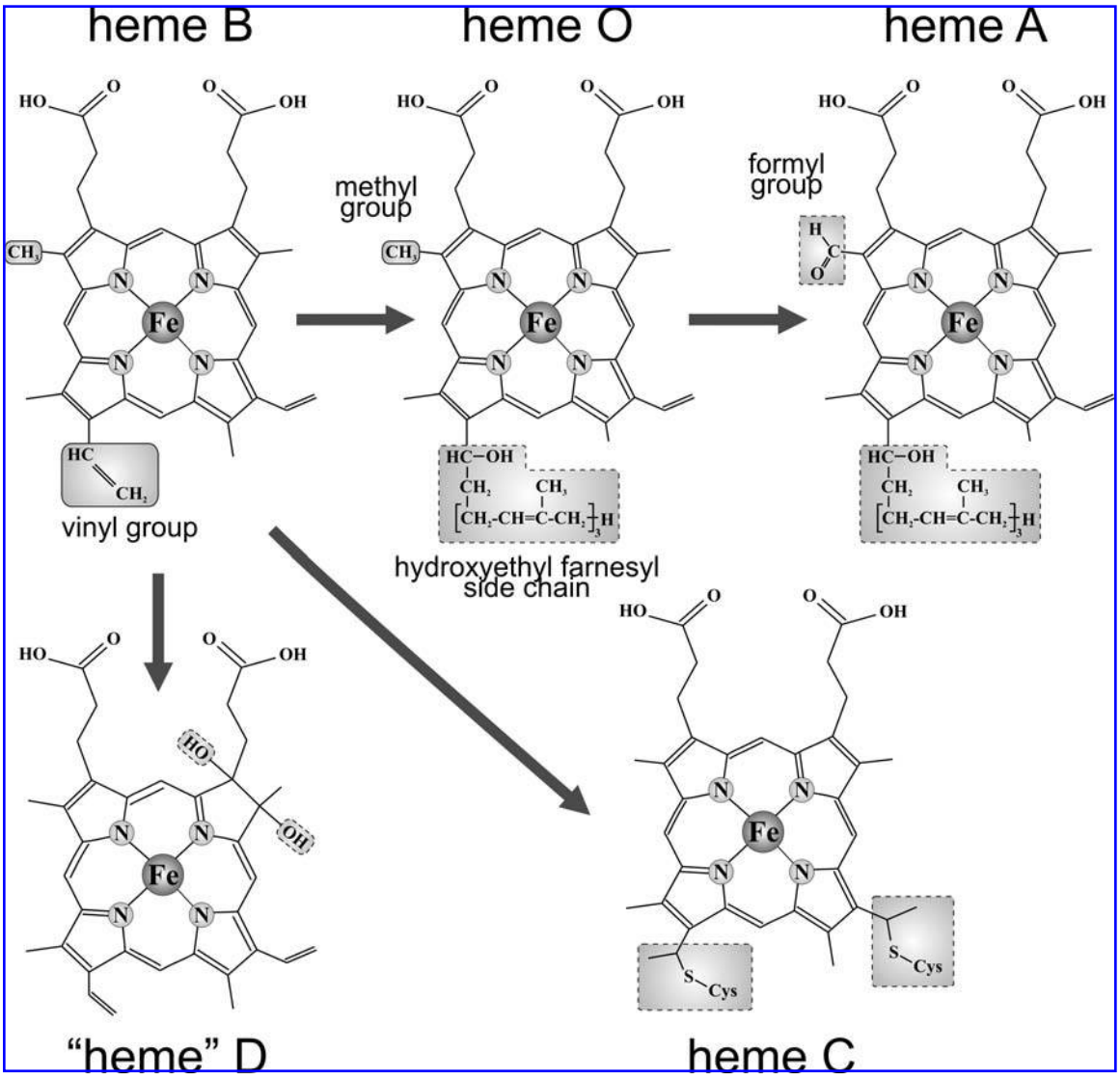

FIG. 3. Structures and biosynthesis of heme B, heme O, heme A, heme D, and heme C. In heme D, one double bond in a pyrrole ring has been reduced, so it is actually a chlorin, rather than a real heme; the structure of heme C is identical to that of heme B, except that heme C is covalently bound to polypeptide *via* thioether bridges.

genases from the strict aerobe *Azotobacter vinelandii* (120) or from some enteric bacteria (94), reduction can be easily inhibited by high concentration of dioxygen. Thus, the oxygen concentration in these organisms must be maintained from one side low enough to allow nitrogen fixation and, from the other side, high enough for adequate synthesis of ATP. It was shown that in these bacteria, cytochrome *bd* is a key element in the respiratory chain, involved in the oxygen-regulating process (94, 120).

Depending on the construction of the catalytic site, terminal oxidases can be divided into two families: the heme-copper superfamily and the cytochrome *bd*–type family. Most terminal oxidases belong to the heme–copper superfamily (70); they are characterized by a unique binuclear catalytic site, where all the chemistry of oxygen reduction to water occurs. The binuclear site is located in subunit I and consists of a high-spin heme and a copper atom, called Cu_B. Both high-spin heme and Cu_B are retained in the protein by ligation with one and three histidine residues, respectively. In addition to the binuclear site, subunit I also contains a low-spin heme, which is ligated by two histidine residues, and serves as a donor of electrons to the binuclear center. Together, the binuclear center and the electron-donating heme form a core element, which is common for all members of the heme–copper oxidase superfamily. In bacteria, heme groups can be presented by different heme types: B, O, or A (Fig. 3) (46). In addition to the core element, some oxidases of this class might have extra prosthetic groups, like a bimetallic copper site Cu_A (in aa_3 type of oxidases) and one *c*-type heme (in caa_3), or even several *c*-type hemes (cbb_3).

Heme–copper oxidases can be divided into two main subgroups based on the source of electrons they are able to use. The first subgroup, cytochrome *c* oxidases, receive electrons from the water-soluble cytochrome *c* and are found in both eukaryotic and bacterial organisms. The most extensively studied examples of these oxidases are mitochondrial CcO from bovine heart; bacterial aa_3-type oxidases from *Paracoccus denitrificans* and *Rhodobacter sphaeroides*; cytochromes ba_3 and caa_3 from *Thermus thermophilus*; and cytochrome cbb_3 from various species. The second subgroup is represented by quinol oxidases, which are found only in bacteria. Quinol oxidases accept electrons directly from quinols in the cytoplasmic membrane. The well-known member of this class is cytochrome bo_3 from *Escherichia coli*.

The second family of terminal respiratory oxidases is *bd*-type quinol oxidases. In contrast to heme–copper oxidases, cytochrome *bd* has a completely different construction of the catalytic site. It lacks a copper atom and is formed most likely by two high-spin hemes: heme *d* (Fig. 3) and heme b_{595}. In addition to these hemes, cytochrome *bd* contains a low-spin heme b_{558}, which is directly involved in the oxidation of quinols (78). Although this oxidase does not pump protons across the membrane (139, 174), it can still create $\Delta\mu_H^+$ by virtue of vectorial chemistry. However, it results in reduced coupling efficiency, which nevertheless has an adaptive importance for bacteria.

IV. STRUCTURE OF CYTOCHROME *C* OXIDASE

A clear understanding of the mechanism of protein function is almost impossible without a knowledge of its 3D structure. The last decade was extremely successful in resolving the structures of membrane-bound proteins by x-ray crystallography. Even though the basic composition of terminal oxidases—mo-

TABLE 1. THE LIST OF RESOLVED CRYSTALLOGRAPHIC STRUCTURES OF TERMINAL OXIDASES

Type	*Source*	*Resolution*	*PDB number*	*Reference*
aa_3	Bovine	2.80 Å	1OCC	220
aa_3	Bovine	2.80 Å	1OCC	221
aa_3	Bovine	2.30 Å	2OCC	265
aa_3-reduced	Bovine	2.35 Å	1OCR	265
aa_3-CO bound	Bovine	2.80 Å	1OCO	265
aa_3-N_3 bound	Bovine	2.90 Å	1OCZ	265
aa_3	Bovine	1.80 Å	1V54	222
		1.80 Å	2DYR	153
aa_3-reduced	Bovine	1.90 Å	1V55	222
		1.90 Å	2EIJ	153
aa_3-Cd^{2+} bound	Bovine	2.1 Å	2EIK, 2EIL	153
aa_3-Zn^{2+} bound	Bovine	2.7 Å	2EIM, 2EIN	153
aa_3	*P. denitrificans*	2.80 Å	1AR1	105
aa_3	*P. denitrificans*	2.70 Å	1AR1	162
aa_3	*P. denitrificans*	3.00 Å	1QLE	85
aa_3	*R. sphaeroides*	2.30 Å	1M56	215
aa_3-E286Q	*R. sphaeroides*	3.00 Å	1M57	215
aa_3	*R. sphaeroides*	2.00 Å	2GSM	177
ba_3	*Th. thermophilus*	2.40 Å	1EHK	211
ba_3	*Th. thermophilus*	2.30 Å	1XME	104
bo_3, quinol oxidase	*E. coli*	3.50 Å	1FFT	2

Three-dimensional structures of terminal oxidases and other biologic macromolecules can be downloaded from RCSB Protein Data Bank (http://www.rcsb.org/pdb).

Table 2. Subunit Composition of Terminal Oxidases in Mitochondria and Bacteria

	Bovine (heart) aa_3			*P. denitrificans aa_3*	
Subunit	M_r	*Composition*	*Encoded by*	M_r	*Composition*
I	56993	12 α-helices	Mitochondria	62500	12 α-helices
II	26049	2 α-helices	Mitochondria	27999	2 α-helices
III	29918	7 α-helices	Mitochondria	30671	7 α-helices
IV	17153	1 α-helix	Nucleus	5364	1 α-helix
Va	12434	At the N-side	Nucleus		
Vb	10670	At the N-side	Nucleus		
VIa	9418	1 α-helix	Nucleus		
VIb	10068	At the P-side	Nucleus		
VIc	8480	1 α-helix	Nucleus		
VIIa	6234	1 α-helix	Nucleus		
VIIb	6350	1 α-helix	Nucleus		
VIIc	5541	1 α-helix	Nucleus		
VIII	4962	1 α-helix	Nucleus		

Mitochondrial subunit nomenclature from (111); molecular masses for bovine aa_3 from (50); molecular masses for *P. denitrificans* aa_3 from (82, 259).

lecular weight and number of subunits, types and quantity of prosthetic groups, sequence, and conserved residues—was already known before the crystal structure came out, the real breakthrough was achieved only when the first crystallographic structures of CcO were resolved (105, 220). At present, the structures of terminal oxidases from five organisms have been resolved, with resolution up to 1.8 Å (Table 1). Nevertheless, even though the structures of CcO in both oxidized and reduced states are known, they appear to be very similar, and the molecular mechanism of CcO functioning is still enigmatic. Solving the structures of all intermediates in the catalytic cycle of CcO can help to answer this question. Unfortunately, the intermediates of the catalytic cycle of CcO are quite unstable, which makes this task extremely difficult, although in some cases, such an approach has provided invaluable information about the mechanism of protein functioning. For instance, the structure of the light-driven proton-pump bacteriorhodopsin was solved in all main states of the photocycle, which made it possible to create a picture of the function of this protein (127).

Mammalian CcO has a molecular mass of ~200 kDa and contains 13 different polypeptide subunits (Table 2). The three largest subunits form a core of the enzyme, encoded by the mitochondrial genome, whereas the remaining 10 subunits originate from nuclear DNA (50). Bacterial CcO (Table 2) are simpler in structure and have only from three to four subunits (Fig. 4A), but the sequence homology of subunits I, II, and III to the corresponding ones of mitochondrial CcO is extremely high (179, 212). The sequence identity between CcO from *R. sphaeroides* and from bovine heart for subunit I is 52% (202); for subunit II, 39% (49); and 50% for subunit III (48). Thus, the bacterial terminal oxidases can be an excellent model for functional studies of more-complex eukaryotic oxidases, mainly because of easier and faster ways of manipulation with the enzyme by molecular genetic methods (102).

A. Subunit I

Subunit I is the largest and the most conserved (197) subunit of CcO, with a molecular mass of ~60 kDa (Table 2). It consists of 12 transmembrane helices without any large extramembrane part (Fig. 4A, shown in light gray). The helices are not perpendicular to the membrane plane but tilted ~20–35 degrees against it. When viewed from the top (P-side), the 12 segments of subunit I are arranged in a counterclockwise direction and form three semicircular arcs, arranged in quasi-threefold axis of symmetry (Fig. 4B). Three pores (pores *A*, *B*, and *C*) are formed in the center of the arcs. Pore *B* houses the binuclear center (heme a_3 and Cu_B) of the oxidase and includes the proton-conductive K channel directed from the binuclear center toward the N-side of the membrane (see later). Pore *C* retains heme *a*; the last pore *A* is empty and used for the proton-conductive D channel as well as for a plausible pathway for oxygen delivery to the binuclear site (189).

Heme *a* is located in pore *C* at a depth of about one third of the membrane thickness from the P-side and oriented perpendicular to the membrane plane, such that its propionates are pointing toward the P-side of the membrane. In both reduced ($S = 0$) and oxidized ($S = {}^1/_2$) states (17, 225), the heme iron is bound to four nitrogens of the porphyrin ring and to two conserved histidines of subunit I. The latter two histidine axial ligands of heme *a,* $His94_I$ ($His61_I$) and $His413_I$ ($His378_I$) (the numbering of amino acid residues is based on the *Paracoccus denitrificans* enzyme; the corresponding amino acid residues in the bovine, *Bos taurus* CcO are shown in brackets), are located in helices II and X, respectively (105, 203, 220); the bonds between the histidines and the heme iron are necessary for holding the heme in the protein.

Biosynthesis of heme A is a sequential process (Fig. 3), and it involves initial farnesylation of protoheme (heme B) at the 2-position (195), forming heme O. In the next stage, the heme O product is modified by hydroxylation of the methyl group at 8-position of the porphyrin ring to formyl (54).

The low-spin hemes in terminal oxidases are responsible for most absorption in the visible part of the spectrum. The decomposed oxidized spectrum of heme *a* has peaks at 426 nm ($\varepsilon \sim 120$ mM^{-1}cm^{-1}, Soret band) and 595 nm ($\varepsilon \sim 19.5$ mM^{-1}cm^{-1}, alpha band) (228). Absorption properties of heme *a* depend on the reduction state of the heme, making this cen-

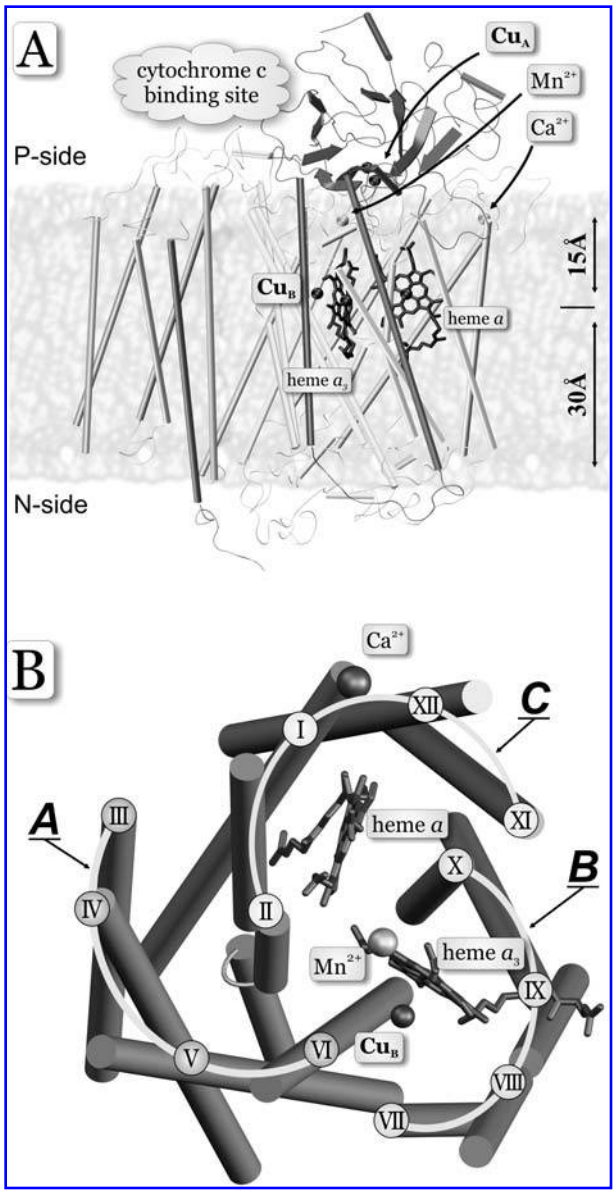

FIG. 4. The structure of cytochrome *c* oxidase from *P. denitrificans*. (**A**) Organization of the subunits and redox-active centers. Hemes and coppers are shown in black (heme a_3 on the left and heme *a* on the right side). Both hemes and Cu_B are situated at the depth of about one third of the membrane from the P-side. (**B**) The top view of subunit I; only metal centers and transmembrane helices are shown. Helices form three semicircular arcs denoted *A* (III-VI), *B* (VII-X), and *C* (I, II, XI, XII).

ter an easy target for optical spectroscopy studies. The reduced-*minus*-oxidized difference spectrum of heme *a*, produced by the ligand-binding method introduced by Horie and Morrison (99), has a peak at 445 nm ($\varepsilon \sim 57$ mM^{-1}cm^{-1}), trough at 425 nm ($\varepsilon \sim -41$ mM^{-1}cm^{-1}) in the Soret region and another peak at 605 nm ($\varepsilon \sim 20.5$ mM^{-1}cm^{-1}) in the alpha region (228). The absorption maximum at 605 nm in the reduced-*minus*-oxidized spectrum of heme *a* in CcO is quite unusual for low-spin A-type heme (132). This maximum is red shifted for ~15 nm compared with an isolated bis-imidazole heme A model compound (47) because of formation of a strong hydrogen bond between the formyl group of heme *a* and neighbor $Arg54_I$ ($Arg38_I$) (113, 131, 191).

The second A-type heme is situated at ~13 Å (center-to-center distance) from heme *a* and is denoted a_3. The plane of heme a_3 is also perpendicular to the membrane, and the propionates point towards the P-side in a manner similar to heme *a*. Both hemes are facing each other at an angle of 104–108 degrees (105, 220). Heme a_3 is a high-spin heme in both the fully reduced *ferrous* state (S = 2) (18) and the resting *ferric* state (S = $^5/_2$) (17). Depending on conditions, heme a_3 can be five- or six-coordinated (17): the permanent bonds of the heme iron include four bonds with nitrogens of the porphyrin ring and one extra bond with the conserved $His411_I$ ($His376_I$) (105, 203, 220). The latter fixes the heme in the protein. Five-fold coordination of the heme iron leaves one side of the heme empty and available for binding of ligands such as dioxygen, carbon monoxide, azide, hydroxide ion, individual water molecules, and so on. The binding of ligands can modulate the spin state of this heme [*i.e.,* binding of cyanide to the ferric form changes the spin-state of heme a_3 from high- to low-spin (S = $^1/_2$) state (17)].

The absolute absorption spectrum of oxidized heme a_3 has a highly pronounced maximum in the Soret region at 414 nm ($\varepsilon \sim 81$ mM^{-1}cm^{-1}) and low-intense bands in the alpha region, including a maximum at ~600 nm and a β-band at ~560 nm (228). The main absorption changes in the reduced—*minus*—oxidized spectrum of heme a_3 also correspond to the Soret region, with a peak at 444 nm ($\varepsilon \sim 112$ mM^{-1}cm^{-1}) and trough at 411 nm ($\varepsilon \sim -50$ mM^{-1}cm^{-1}), whereas the absorbance in the alpha region is much less pronounced, with a single peak at ~601 nm ($\varepsilon \sim 4.9$ mM^{-1}cm^{-1}) and a shoulder at ~579 nm ($\varepsilon \sim 3.9$ mM^{-1}cm^{-1}) (133, 228). In addition, oxidized heme a_3 has one extra band detected at ~655 nm (*charge-transfer* band) attributed to charge-transfer to a ligand of heme a_3 (21, 143, 204).

The last redox metal center of subunit I is ~5 Å away from heme a_3 iron and is formed by a copper atom denoted Cu_B. Together, heme a_3 and Cu_B form the binuclear catalytic center of the oxidase (Fig. 5), where all the chemistry of dioxygen splitting and reduction to water take place. The distance between the heme a_3 iron and Cu_B seems to be the same in both reduced and oxidized states of the enzyme (85) or slightly fluctuates in a range of ~0.1–0.3 Å (222, 265). The oxidized Cu_B is a tetragonal center (65); it has three permanent axial histidine imidazole ligands, identified by both genetic (102) and x-ray spectroscopic approaches (105, 162, 220), as well as one mobile oxygen ligand with exchangeable proton/protons (65). The imidazole ligands originate from $His276_I$ ($His240_I$) in helix VI, and from $His325_I$ ($His290_I$) and $His326_I$ ($His291_I$), both located in a loop fragment between helices VII and VIII.

Because of an extremely low extinction coefficient, the absorbance spectrum of Cu_B is still unknown, although it is possible to obtain information about the redox state of this center by optical spectroscopy. Existing data indicate that the appearance of the *charge-transfer* band (655 nm) requires oxidation of both components of the binuclear center; so reduction of Cu_B, when heme a_3 is oxidized, will induce decay of intensity of the *charge-transfer* band (21, 143). The other technique to detect the Cu_B center is electron paramagnetic resonance (EPR) spec-

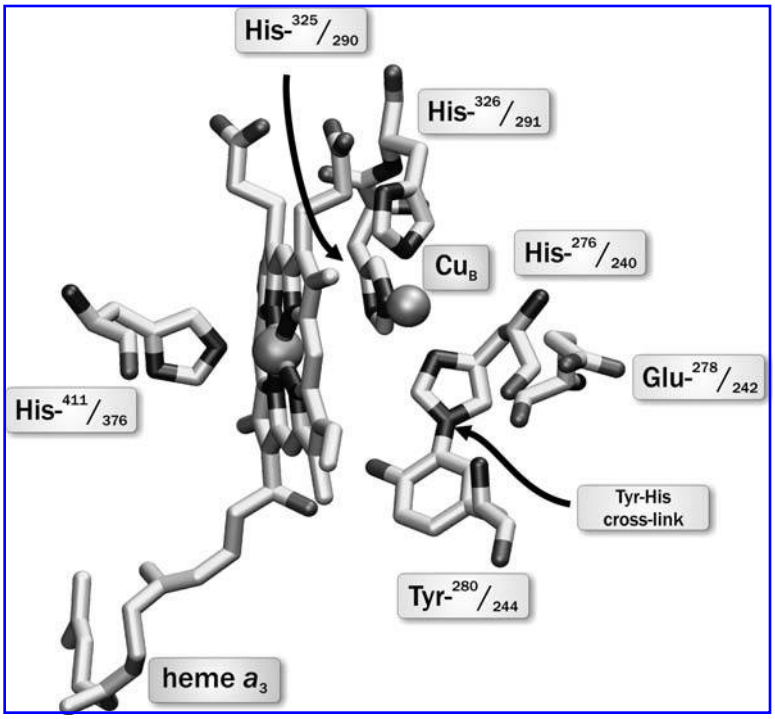

FIG. 5. Catalytic center of cytochrome *c* oxidase: high-spin heme a_3, Cu_B, histidine-tyrosine cross-linked structure, and their ligands. Amino acid numbering from *P. denitrificans*/bovine enzymes.

troscopy, which allows studying molecules and ions with unpaired electrons. Because in the oxidized state, the copper atom contains one unpaired electron on the highest orbital, in theory, the redox state of Cu_B can be followed by EPR. Unfortunately, the presence of the heme a_3 iron in proximity to the copper atom results in a strong antiferromagnetic interaction between these two centers, making them both EPR silent (227) in most situations. Only when either of them is reduced or the magnetic coupling has been broken by other means, the EPR signal from the oxidized center will appear. On some special occasions, the EPR signal (four sharp peaks centered at about g = 2.25) assigned to Cu_B can be seen [*e.g.*, in a reaction of the fully-reduced CcO with dioxygen done at low-temperature (32, 114, 115, 149, 181)], or by decoupling of the heme a_3-Cu_B pair by using different techniques: ligand binding, gamma radiation, saturated ammonium sulfate treatment, incubation in some detergents, and so on (166).

Another important structure identified in CcO is represented by the covalently bound $His276_I$ ($His240_I$) and $Tyr280_I$ ($Tyr244_I$) (Fig. 5). The three histidines and the tyrosine form a conjugated π-electron system around the Cu_B center. In addition to crystallographic studies, the existence of the histidine-tyrosine crosslink was also confirmed by protein-sequencing and mass-spectroscopy analysis of CcO from several species (43, 180). Formation of this bond might considerably reduce pK_a of the tyrosine (137, 265), allowing it to participate in the oxygen-reduction process by donating both the proton and the fourth electron required for the reaction, thereby forming a tyrosine radical (172, 173).

Besides the redox-active centers, subunit I also contains tightly bound non-redox active metal centers. The Mg^{2+}/Mn^{2+} binding site is located at the interface between subunit I and II, approximately halfway between the heme a_3 and Cu_A centers. The metal atom is ligated to $His403_I$ ($His368_I$), $Asp404_I$ ($Asp369_I$), $Glu198_{II}$ ($Glu218_{II}$), and to three water molecules (101, 162, 215, 220, 265). In mitochondrial CcO, this site is occupied by magnesium (61, 220), whereas in bacterial oxidases, it can be partially substituted by manganese atom (200). The function of this metal site is unknown, but it was shown that Mn^{2+} is located in the expulsion pathway for the water molecules that are produced in the binuclear center of the oxidase (199). However, the site-specific mutagenesis of the metal-ligating residues revealed neither change in pumping efficiency nor significant decrease in enzymatic activity (67, 101). In addition, proton-translocating quinol oxidases lack this center (2) without any effect on the ratio of proton translocation (175, 232). Both subunit I and II have a number of negatively charged residues at the interface between them, and the Mg^{2+}/Mn^{2+} site may be important for their stabilization.

Another nonredox active metal site was found in a loop between helices I and II close to the P-side of the membrane. The identity of a metal ion in this center is not completely clear: based on ligand coordination pattern, it is assigned to be occupied by sodium in mitochondrial oxidases (265) or by calcium in bacterial ones (162, 215). At the same time, cation-binding experiments suggest that in the mitochondrial CcO, this site reversibly binds calcium or sodium (121), whereas in bacterial oxidases, this site contains only tightly bound calcium that cannot be removed by an excess of chelating agents such as EGTA (130, 167, 188). The role of the tightly bound Ca^{2+} can be in the structural stabilization of oxidases (130).

B. Subunit II

Subunit II is another subunit of CcO, which contains redox active cofactors. It has a molecular mass of ~27 kDa (Table

2), and it forms two transmembrane helices interacting with subunit I (Fig. 4A) and a large C-terminal hydrophilic globular domain at the P-side of the membrane (105, 221). The redox active copper center, conventionally referred to as Cu_A, is formed by two copper atoms. A long discussion has been held in the oxidase field concerning the type and number of copper atoms in the Cu_A center, and only at the beginning of the 1990s was this issue finally resolved (11, 119, 125, 128, 135, 226). The Cu_A center in the oxidized state of the enzyme was found to be in mixed-valence configuration that can be formally represented as $[Cu^{1.5+}\text{-}Cu^{1.5+}]$. On reduction Cu_A holds an electron by sharing it between both copper atoms. This redox center is situated in the globular domain almost on the border with subunit I. As was shown by site-directed mutagenesis (119) and confirmed later by x-ray crystallography (105, 220), Cu_A is ligated to two cysteines [$Cys216_{II}$($Cys196_{II}$) and $Cys220_{II}$($Cys200_{II}$)], two histidines [$His181_{II}$($His161_{II}$) and $His224_{II}$($His204_{II}$)], one methionine [$Met227_{II}$($Met207_{II}$)], and one carbonyl oxygen of $Glu218_{II}$ ($Glu198_{II}$).

The redox state of Cu_A can be followed by optical absorbance spectroscopy. The spectrum of oxidized Cu_A has two clear maxima: a broad peak at ~820 nm ($\varepsilon \sim 1.6$ mM^{-1}cm^{-1}) and a rather sharp peak at 480 nm ($\varepsilon \sim 3.0$ mM^{-1}cm^{-1}) with a shoulder at ~530 nm (107, 128). Even though the extinction coefficient of the latter peak is higher, the practical characteristic wavelength of Cu_A in the intact CcO is in the region of ~820 nm, where hemes do not absorb light, thus making it possible to follow redox changes of Cu_A only. In addition to optical absorbance spectroscopy, the EPR technique proved to be a valuable tool for studies of Cu_A. Oxidized Cu_A possesses a strong and characteristic EPR signal in the g ~ 2 region (1, 22) measured at the temperature of liquid nitrogen and lower.

C. Subunit III

Subunit III is the biggest subunit of CcO that has no redox cofactors. It has a molecular mass of ~30 kDa (Table 2) and consists of seven transmembrane helices without any extensive extramembrane domain. The helices of subunit III are arranged into two bundles: the first one is formed by helices I and II, and the other, by helices III to VII (105, 221). The bundles of helices are tilted against each other forming a big V-shaped cleft between them with a bottom at the N-side of the membrane. Subunit III is in side-to-side contact with the helices of pore A of subunit I.

The function of this subunit is unknown: it contains no prosthetic groups, and it is not involved in proton pumping, as was shown on two-subunit enzyme from *P. denitrificans* reconstituted into liposomes (87, 210) and by mutagenesis study (81). However, it might be involved in the stabilization of a mature oxidase and in ensuring correct assembly of the enzyme (especially at the final folding step of subunit I), including structural adjustment of heme centers (80). At the same time, the V-shaped cleft is located at the mouth of the oxygen-conducting channel and may secure the constant flux of oxygen into the catalytic center (189) (see later). It is also possible that the membrane-anchored cytochrome c_{552}, which is a physiologic electron donor for CcO from *P. denitrificans* (27), might use this cleft for binding and placing itself in an appropriate position for electron transfer to Cu_A (105).

D. Other subunits

In addition to three core subunits, the heme–copper terminal oxidases can have extra subunits. CcO from *P. denitrificans* has one additional subunit (82, 105) with a molecular mass of ~5 kDa (259). It has one transmembrane helix, which is in contact with all other subunits. The function of this subunit is unknown: the deletion of its gene has no effect on either protein integrity or enzymatic and spectral properties of the oxidase (259).

In mammalian CcO, the three mitochondrially encoded core subunits (homologous to the three main subunits of the bacterial enzyme) are supplemented by ten additional subunits, which are encoded by nuclear DNA (Table 2). Seven of ten nuclear-encoded subunits consist of one transmembrane helix each, whereas subunits Va, Vb, and VIb are represented by small globular proteins. Subunits Va and Vb are bound to the oxidase at the matrix side of the protein, whereas subunit VIb is bound at the intermembrane side. Because none of the nuclear-encoded subunits is associated with the active site, it is quite unlikely that they are important in the functional mechanism of CcO. However, based on findings of binding sites for ATP/ADP (110, 221), protein kinase A (263), and 3,5-diiodothyronine (14) within some of them, it is assumed that the nuclear-encoded subunits have a regulatory function. The role of these subunits in the regulation of the enzymatic activity is also supported by the presence of their tissue-specific isoforms in mammals (110). Studies on subunit VIb from yeast, which is highly identical to bovine CcO, show that this subunit can be important during assembly of the oxidase, although it can be removed from the mature enzyme without any effect on activity (126). The crystal structure of bovine CcO indicates that subunits VIa and VIb might be involved in stabilization of a dimer state of the protein (221). In addition, mitochondrial oxidase contains Zn^{2+}, which is tightly bound to subunit Vb (220, 221).

V. TRANSIENT KINETICS APPROACH FOR INVESTIGATION OF THE ENZYME CATALYTIC CYCLE

A. Methodologic approaches

The typical rate of oxygen reduction by CcO under steady-state conditions is ~100– 200 enzyme revolutions per second. This implies that the single turnover of the protein is extremely fast and occurs in the milliseconds time domain. At the same time, each turnover has a number of distinct intermediates, which are formed in microseconds to several milliseconds from the beginning of reaction. Thus, because of a large number of catalytic intermediates, complicated by a large hierarchy of transition-rate constants between them, it is impossible to study the mechanism of CcO functioning by means of conventional steady-state techniques. The main problem in the steady-state approach is that, under such conditions, only the longest-lived intermediate is populated, leaving all other intermediates completely invisible. The transient kinetics approach makes it possible to overcome these difficulties but requires a certain number of conditions that must be fulfilled.

- First, the measuring system must allow time resolution faster than the fastest reaction step under investigation. This is actually the least difficult matter now because of developments in the field of modern electronics (*e.g.,* development of the CCD, fast analog-to-digital converters, and powerful computers for real-time processing).
- Second, the sample solution consists of a very large quantity of individual protein molecules that function independently, and it is very important to set all of them into the same state before initiation of the reaction.
- Third, addition of substrates to the enzyme must be carried out faster than the fastest transition under investigation. This is a real challenge because the fastest mixing time of a conventional stopped-flow apparatus is in the range of milliseconds, which is much slower than most of the intermediate transitions in the catalytic cycle. A possible solution to this problem is to start the reaction by immediate enzyme activation (for example, by a laser flash).

Even though the catalytic reaction of CcO consists of electron and proton transfers together with oxygen-reduction chemistry, it is controlled by electron entry into the enzyme. In general, electron transfer can occur in two opposite directions: *to* and *from* the binuclear center. In the first case, the movement of electrons coincides with the normal physiologic direction of electron transfer, whereas the other case is an artificial experimental model for detailed studies of electron-transfer reactions (*backflow* reaction).

Two main approaches were introduced for measurements of the catalytic reactions in CcO in real time. One of them, the *flow-flash* method (73), is a combination of the conventional stopped-flow technique with laser-induced initiation of the reaction. In this method, instead of straight mixing of the fully reduced CcO with dioxygen, the protein is first allowed to react with carbon monoxide, which binds at the oxygen-binding site to the reduced heme a_3; after that, the CO-bound oxidase is mixed in a stopped-flow apparatus with an oxygen-containing buffer. Under these conditions, the reaction of dioxygen with the CO-bound oxidase is limited by the CO-dissociation rate [*ca.* 0.02/sec (73, 74)], but at the same time, the Fe–CO bond is photolabile and can be instantly photolyzed by a laser flash. The laser flash photolyzes CO from heme a_3 allowing dioxygen to bind and begin the reaction. The following transitions can be monitored by a number of different time-resolved detection techniques such as optical absorption spectroscopy (30, 73, 90, 91, 93, 157, 161, 214, 238, 241), potentiometric electrometry (108, 235, 239), resonance Raman (84, 156, 229–231) and so on. The flow-flash method is very useful; however, its scope is severely restricted by a limited number of starting conditions, and it is normally used for studying the oxidative part of the catalytic cycle only. In addition, the beginning of the reaction is complicated by the phase of CO release, which takes the same route *via* Cu_B (8) as subsequent dioxygen binding (241). Fortunately, CO dissociation from the binuclear center seems to be much faster (261) than the following step of oxygen binding and should not affect it.

The second approach is the initiation of the reaction by the injection of a single electron into the enzyme. The most successful implementation has been the use of photo-activated ruthenium derivatives (23, 33, 72, 155, 194, 207, 244, 266, 267), such as tris(2,2′-bipyridyl) ruthenium (RubiPy) for the reaction initiation in CcO. Under low-ionic-strength conditions, RubiPy binds electrostatically to the oxidase at the cytochrome *c*–binding pocket. A laser flash turns the molecule of RubiPy into an excited state with an E_m of about −1.5 V, which donates an electron to Cu_A in less than 0.5 μsec. The injected electron is further redistributed among all redox cofactors according to their midpoint potentials. The reverse reaction of enzyme reoxidation by the oxidized RubiPy is prevented by addition of a sacrificial electron donor, like, for example, aniline or EDTA. Electron injection is a very powerful and useful technique, albeit with certain limitations: the main one is a relatively small quantum yield, which is typically less than 10%.

An alternative way to study electron transfer in CcO is investigation of the electron *backflow* reaction and processes coupled to it by the *perturbed equilibrium* method. In this method, binding of CO to the partially reduced oxidase increases the apparent midpoint potentials of heme a_3 and Cu_B, trapping electrons at the binuclear center. The bound molecule of CO can be dissociated away by a flash of light, causing electron redistribution among all redox centers according to the new redox equilibrium (section VII).

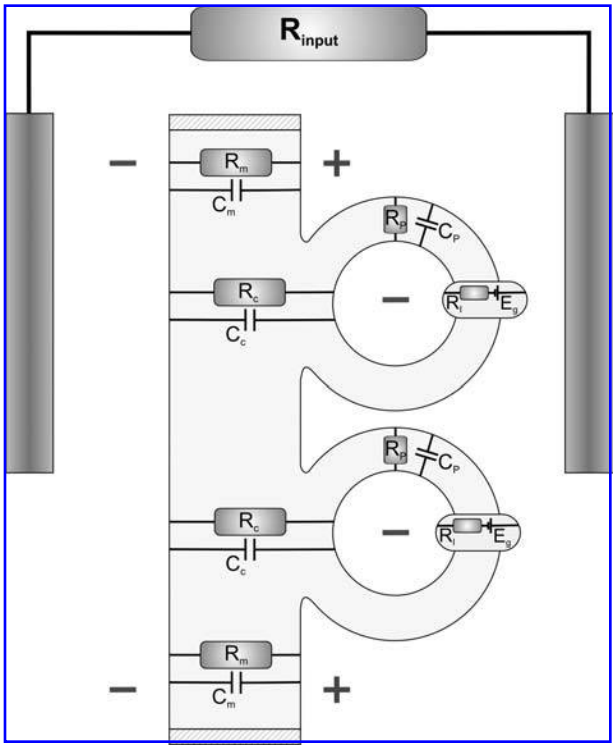

FIG. 6. Scheme of the electrometric setup. CcO is reconstituted into phospholipid vesicles that are fused to the phospholipid-measuring membrane. The electrode potential measured by Ag/AgCl is proportional to the potential generated by the enzyme. C_m, C_p, and C_c are the capacitances of the measuring membrane, the liposomal membrane, and their contact, respectively. R_m, R_p, and R_c are the corresponding resistances. R_i is internal resistance, and E_g is the electromotive force of the molecular generator.

B. Time-resolved potential electrometry

The functioning of CcO is directly linked to the translocation of both electrons and protons across the membrane. Whereas the transfer of electrons can be relatively easily monitored by different spectroscopy methods, the time-resolved transfer of protons can conveniently be detected by potential electrometry. Potential electrometry is a method of direct measurement of electric-charge translocation by membrane proteins. It was originally developed for bacterial reaction centers and bacteriorhodopsin (58, 59), but later also applied for CcO (266). In recent years, the method has advanced extensively, allowing detection of $\Delta\Psi$ generated not only in the light-induced reactions, but also after addition of other substrates such as O_2 or NO (88, 239). The idea of the method is that, first, the molecules of CcO are incorporated into phospholipid vesicles by gradual removal of detergent from the protein/lipid mixture (96, 186). Then the vesicles with CcO are fused to the planar phospholipid-measuring membrane because of neutralization of negative charges on the membrane surface by Ca^{2+} or Mg^{2+} ions (Fig. 6). The measuring membrane should be very thin to possess large electric capacitance for the recording of fast charge translocation. During the enzymatic reaction, CcO creates $\Delta\Psi$ on the vesicle membrane, which is then proportionately divided with the measuring membrane and thus can be detected by Ag/AgCl electrodes situated on its different sides. Typically, the measuring membrane has high resistance of ~1–5 GOhm, and the measured $\Delta\Psi$ decays with a time constant of several seconds.

This method is extremely sensitive, allowing detection of charge translocation of <1 Å across the membrane dielectric in the direction perpendicular to the membrane plane. But at the same time, it has certain limitations natural for any vesicle-related technique; for instance, the orientation of protein molecules may be stochastic, decreasing the amplitude of the signal, or the substrate binding sites might be unreachable if they are located on the inner side of the vesicle membrane.

VI. PATHWAYS AND REDOX COFACTORS OF CYTOCHROME *C* OXIDASE

The chemical reaction of oxygen reduction to water, which triggers proton translocation across the membrane, occurs at the binuclear center in the middle of the protein and requires both delivery of substrates (*i.e.,* electrons, protons, and oxygen) and release of products (water). All these aforementioned reagents that are necessary for oxidase functioning are transported toward the catalytic site through especially designed pathways. These pathways have been identified, and they can be divided into electron-, proton-, and oxygen-transfer structures.

A. Electron-transfer pathways

The transfer of electrons inside proteins is a quite complicated process defined by a number of factors. According to electron-transfer theory (136), the rate of electron transfer depends on the distance between donor and acceptor, the difference in their redox potentials, and the reorganization energy (*i.e.,* the energy required to alter the equilibrium geometry of the initial state into the equilibrium geometry of the product). Two main theories describe how the electron is transferred within a protein. In the first conceptualization (77), the electron tunneling is considered to occur specifically through bonds and can be modulated by conformational changes of the secondary structure of the protein. In contrast, the other theory (152, 163) postulates that the efficient tunneling of electrons is not limited to any specially designed pathway within the protein, but rather occurs *via* multiple pathways through the protein medium; in the simplest view, it can be defined by edge-to-edge distance between donor and acceptor, modified by the atomic density of the intervening medium.

The reduction of dioxygen to water requires four electrons. These electrons are donated one by one from a water-soluble cytochrome *c*, which serves as one-electron transfer mediator between bc_1-complex and CcO. Cytochrome *c* binds to a cleft between subunit II and III at the P-side of the membrane (69, 105). This area is enriched with acidic residues (105, 221) that could interact with positively charged lysines and arginines on the surface of cytochrome *c* (44, 185). Thus, it is likely that the formation of a cytochrome *c*–CcO complex is defined mostly by electrostatic interactions between the proteins; this fact is supported by a strong dependence of the reaction of reduced cytochrome *c* with the oxidase on the ionic strength of the medium (10, 86, 260, 269). However, it cannot be excluded that the complex formation is additionally modulated by hydrophobic forces (165). As soon as cytochrome *c* binds to the oxidase, the electron is rapidly transferred to the primary electron acceptor—the bimetallic copper center, Cu_A (90, 122) (Fig. 7). This electron transfer is modulated by the highly conserved $Trp121_{II}$ ($Trp104_{II}$) (260, 269), and the rate of this process is found to be of the order 0.6 to 1×10^5 per second (72, 90, 91).

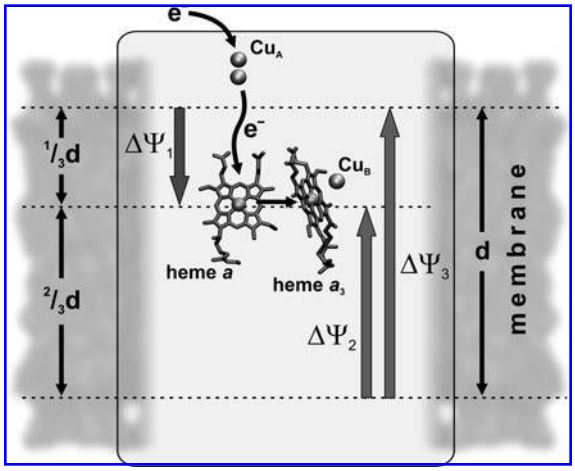

FIG. 7. Relative arrangement of the redox cofactors within the protein. Bold plain arrows perpendicular to the membrane show the direction of charge movements that can be followed with an electrometric setup. $\Delta\Psi_1$, An amplitude of potential generation due to electron movement from Cu_A to heme *a*; $\Delta\Psi_2$ and $\Delta\Psi_3$, due to translocation of a substrate and pumped protons, respectively.

Cu_A is situated near the membrane surface on the P-side of the membrane, whereas all other redox centers are buried at equal depth approximately one third (13 Å) of the membrane thickness below the membrane surface on the P-side (105, 220). The center-to-center distance between Cu_A and the iron atom of heme *a* is 19.5 Å, and this is only 2.6 Å closer than the distance between Cu_A and the iron atom of heme a_3 (22.1 Å). However, despite such similarity in distances, the preference in electron transfer from Cu_A is completely shifted to heme *a*. The reason for this effect may be purely thermodynamic. The electron transfer from Cu_A to heme *a* is not coupled to proton uptake to compensate the negative charge at the heme *a*; at the same time, the midpoint redox potential of heme a_3 without protonation is far too low to permit electron transfer (144, 234); thus, slow protonation may limit the rate of heme a_3 reduction (41, 242), thereby leading to the observed results.

From electron-injection experiments, the rate of electron equilibration between Cu_A and heme *a* is estimated to be $\sim 1.8 \times 10^4$/sec in mitochondrial (72, 122, 155, 266) and $\sim 1.1 \times 10^5$/sec in bacterial oxidases (23, 123, 244, 267). The same equilibration, measured by perturbed equilibrium methods, has similar rates for the mitochondrial enzyme (108, 148, 159, 240), whereas in bacteria, it seems to be three- to fourfold slower at $\sim 2.8 \times 10^4$/sec (3, 25).

Heme *a* serves as a donor of electrons to the heme a_3-Cu_B center. The planes of both hemes are perpendicular to the membrane, forming an interplanar angle of 104 to 108 degrees, with a minimal edge-to-edge distance between the hemes of ~4.7 Å (105, 220). The measured rate of electron equilibration between heme *a* and heme a_3 significantly varies, depending on the particular circumstances under which the measurements are done. When the electron is injected into the oxidized enzyme from reduced cytochrome *c*, the equilibrium can be achieved with a time constant on the order of 0.3–1.0 sec (10); alternatively, when fully reduced oxidase reacts with dioxygen, electron equilibration is much faster and has a time constant of ~30 μsec (90, 241). The fastest rate of electron equilibration between the hemes can be measured after CO photodissociation from the mixed-valence (two-electron reduced) enzyme. In this case, ultrafast electron equilibration between the hemes with $\tau \sim 1.2$ nsec occurs immediately after CO dissociation from heme a_3 (159, 169, 236, 240), and is followed by a slower equilibration phase with τ of ~3 μsec (3, 63, 159, 240), possibly determined by the kinetics of CO dissociation from the Cu_B center (see details later). Such a large magnitude of difference from nanoseconds to seconds in the observed rates of electron equilibration between the hemes is attributed to possible structural rearrangement of the protein or to coupling of electron transfer to protonation or ligand state change of neighboring groups (40, 169, 236, 242).

B. Proton-transfer pathways

Because redox centers of the oxidase are buried within the protein, they have no contact with the aqueous phase. However, maintenance of great rates of respiration requires both fast proton delivery to the catalytic center and corresponding fast proton translocation across the membrane. It should be noted that the proton-transfer pathways in CcO have been much less investigated than the electron-transfer pathways. The protein medium itself cannot facilitate proton delivery toward the binuclear center, or across the membrane, and to overcome this limitation, the oxidase has specially designed proton-conductive structures. It is proposed that these structures are based on chains of hydrogen bonds between hydrogen-bonding protein side groups (polar or protonatable or both) and water molecules, in which the proton is transferred by a Grotthuss-type mechanism (7, 57, 154) (see Fig. 8).

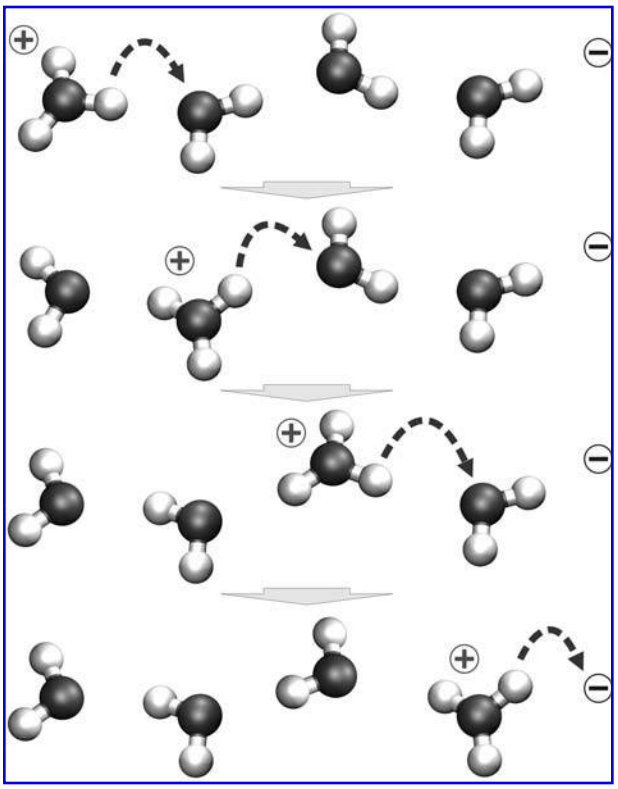

FIG. 8. Proton translocation through a chain of water molecules by the Grotthuss mechanism. Proton denoted + travels to a proton acceptor denoted—by sequential hopping from a hydroxonium ion to an adjacent water molecule.

At least two proton-conductive channels have been identified by site-directed mutagenesis (67, 102, 218, 219) and later confirmed by x-ray spectroscopy (2, 105, 215, 221). Both channels are situated in subunit I of the oxidase and lead from the N-side of the membrane toward the catalytic center of the oxidase (Fig. 9).

One of them is the K pathway after highly conserved lysine 354_I(319) (102, 218), which is situated approximately halfway through the channel. This pathway starts with either $Ser291_I$(255) (105, 221) or $Glu78_{II}$(62) (39, 112, 134) and continues through conserved residues $Lys354_I$(319) and $Thr351_I$(316) toward the hydroxyethyl farnesyl side chain of heme a_3 and $Tyr280_I$(244) in the proximity of the binuclear center. $Tyr280_I$, at the end of the K-pathway, is covalently linked to $His276_I$(240) by a posttranslational modification and is assumed to be involved in oxygen-reduction catalysis. The importance of $Tyr280_I$ is supported by site-directed mutagene-

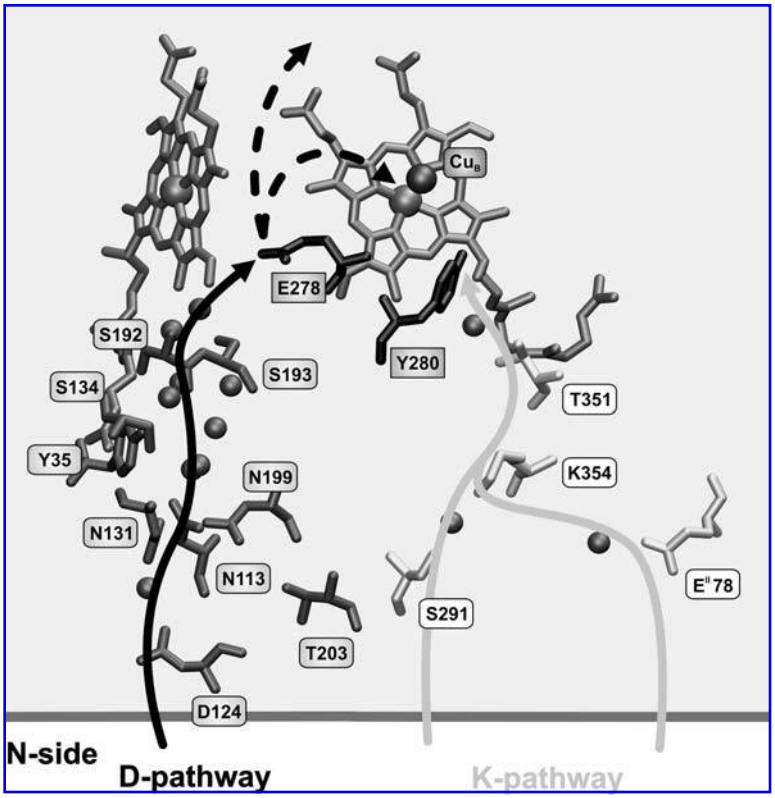

FIG. 9. Proton-conducting pathways together with the redox centers of cytochrome *c* oxidase. The spheres are structurally identified water molecules (based on the bovine 1V54 x-ray structure). The D channel begins from Asp_I124 and leads to Glu_I278; from here, depending on the orientation of the water molecules, it can be directed toward the "pump site" or to the catalytic center. Two possible entrances to the K channel are shown. One starts from Ser_I291, whereas the other is assumed to begin from $Asp_{II}78$. Regardless of its starting point, the K channel leads to conservative lysine 354 and on farther to the binuclear center. *P. denitrificans* amino acid numbering.

sis studies, in which all mutational substitutions for this tyrosine result in complete elimination of oxidase activity (102, 168, 217). Two or three tightly bound water molecules belonging to the K pathway can be found in the x-ray structures. One water molecule is situated between $Thr351_I$ and the hydroxyl group of hydroxyethyl farnesyl side chain of heme a_3, the other between $Ser291_I$ and $Lys354_I$, and the last one is possible between $Glu78_{II}$ and $Lys354_I$ (in 1V54, 1V55; Table 1). The amino acid residues of the K pathway are connected by hydrogen bonds; however, this connection seems to be interrupted by a large hydrophobic gap between $Lys354_I$ and $Thr351_I$, where no water molecules have been found so far. It is proposed that this gap might be bridged by a movement of lysine residue (98).

The other channel, named D after the highly conserved $Asp124_I(91)$ (67, 168, 219), is situated near the surface of the enzyme on the N-side. $Asp124_I$ together with $Thr203_I(167)$ and $Asn199_I(163)$ form a mouth that leads *via* polar residues $Asn113_I(80)$, $Asn131_I(98)$, $Tyr35_I(19)$, $Ser134_I(101)$, $Ser192_I(156)$, $Ser193_I(157)$, and crystallographically identified bound water molecules to $Glu278_I(242)$, which is an important residue for proton pumping (5, 123, 216, 233). The method of proton translocation after $Glu278_I$ is not clear because no proton connectivity beyond this residue was detected in the crystallographic structures. However, it is proposed that this place is occupied by three or four mobile water molecules (187, 270) that form a proton-conductive pathway directing protons either to the Δ-propionate of heme a_3 for pumping or to the binuclear center for water formation (98, 254). Release of the pumped proton out of the enzyme occurs through the highly hydrophilic domain above the heme groups. This area contains an extended hydrogen-bonded network of charged and polar amino acid residues, the propionates of the hemes, bound metal centers, and water molecules, and presumably is involved in the transfer of pumped protons toward the P-side of the membrane (105, 162, 221). Based on results of site-directed mutagenesis studies, it is assumed that the exit channel for pumped protons may start at conserved $Arg473_I(438)$ and $Arg474_I(439)$ (36, 176), which are hydrogen-bonded to the Δ-propionates of the hemes, and then continues farther through the chains of mobile water molecules.

The presence of two independent proton-conducting pathways in the oxidase was suggested immediately after the discovery of proton pumping (15, 253). Later, when the first crystallographic structures of the oxidase were resolved, existence of the channels was indeed confirmed; however, the role of these channels was misinterpreted. Originally, the presence of two channels in the oxidase was explained in terms of a different role for each channel in the proton-transfer mechanism. It was proposed that the D channel is responsible for translocation of "pumped" protons, whereas the K channel is used for uptake of "chemical" protons for water formation (105). However, more recent results indicate that the D channel is involved in the uptake of all four pumped protons and two chemical protons used in the oxidative part of the catalytic cycle (5, 123), whereas the K channel is responsible for the uptake of another two chemical protons during the reductive part of the cycle (6, 33, 103, 123, 250). In addition, $Lys354_I$ may be involved in the oxidative part of the cycle (38), providing charge compensation on electron transfer from heme *a* to the binuclear site and formation of the **P** intermediate.

Interestingly, based on structure analysis of bovine heart CcO in the reduced and oxidized states, one additional proton-conductive pathway was proposed (221, 265). This so-called H channel, after partially conserved $His413_I^{bovine}$, begins at the N-side of the membrane and leads to $Asp51_I^{bovine}$ on the P-side. Depending on the reduction state of heme *a*, $Asp51_I^{bovine}$ changes its conformation (being in protonic equilibrium with the matrix space, when heme *a* is oxidized, and with the intermembrane space when heme *a* is reduced), providing the gate for proton translocation across the membrane. Replacements, by using a bovine gene expression system, of amino acid residues involved in the formation of this channel (like $Asp\text{-}51_I$ to asparagine) abolish the pumping without impairment of the catalytic activity (205, 222). However, it seems that this channel (if any) is a strict property of mammalian oxidases, because bacterial oxidases lack some of the key residues involved in its formation, and extensive mutations of other residues in the proposed area have shown their functional insignificance for proton translocation (131, 168). Thus, either the mechanism of proton pumping in the mammalian CcO is different from the bacterial one, which seems quite unlikely because of their similar properties and structures, or the H channel has another function (for example, charge compensation on heme *a* reduction).

C. Oxygen-transfer pathways

As a small, uncharged molecule, dioxygen can easily permeate membranes and so can reach the catalytic site of the oxidase even without any specific route through loosely packed regions by using conformational fluctuations of the protein. However, the rate of such uncontrolled diffusion is rather slow and most likely insufficient to maintain normal catalytic activity of the oxidase. Thus, the protein must have certain structures that can be used as channels for oxygen delivery to the reaction center. And indeed, analysis of x-ray crystal structures (215, 221), supplemented by experimental (189, 190, 196) and theoretic examinations (98), shows from one (in *P. denitrificans*) to three (in bovine) highly hydrophobic passages from the middle of the membrane bilayer, where oxygen is concentrated, toward the active site. Interestingly, even a single amino-acid mutation can dramatically influence the binding of oxygen from partial [in Val279Ile mutant (189, 190)] to complete inhibition [in Gly283Val mutant of *R. sphaeroides* (196)].

VII. ELECTRON BACKFLOW REACTION

The reaction of the enzyme with oxygen is a complex process that includes electron transfer, proton transfer, and the chemistry of oxygen reduction arranged in a multistep catalytic cycle. From that point of view, study of the electron backflow reaction (34) gives a unique possibility of measuring pure electron-transfer steps in the enzyme.

Under anaerobic conditions, a molecule of CO binds to the reduced heme a_3 instead of oxygen and significantly increases the midpoint potentials of heme a_3 and Cu_B, trapping electrons at the binuclear center (Fig. 10). The heme a_3–CO bond is photolabile and can be broken by a laser flash. With the flash, in several hundreds of femtoseconds, CO leaves heme a_3 and transiently binds to Cu_B (62, 261). After CO dissociation, the midpoint potential of heme a_3 returns to its original value, and the electron is equilibrated between redox centers (3, 25, 60, 108, 148, 159, 240) according to their midpoint potentials.

From optical absorbance measurements, a phase with $\tau \sim 3$–5 μsec was identified and assigned to electron transfer from heme a_3 to heme *a* (3, 63, 159, 240). Surprisingly, the rate of this process is at least three orders of magnitude slower than predicted by electron-transfer theory (152, 163). Recently, the theoretical prediction was confirmed by a quantitative approach (236) and by direct time-resolved measurements by using sensitive pump-probe transient absorbance spectroscopy with femtosecond time resolution (169). Thus, dissociation of CO from the binuclear center (Fig. 10) induces ultrafast electron equilibration between the hemes with $\tau \sim 1.2$ nsec, followed by a slower equilibration phase with $\tau \sim 3$ μsec, which is possibly determined by the kinetics of CO dissociation from the Cu_B center (169, 236), which further reduces the redox potential of heme a_3.

The next transition step happens in 30–50 μsec and includes further electron equilibration between the hemes and Cu_A. In the mixed-valence state, the extent of electron transfer to Cu_A in the 50-μsec phase is negligible (108), but with reduction of the enzyme, it increases, driven by strong anticooperative redox interaction between the hemes, reaching the maximal amplitude at about the three-electron reduction level. On additional reduction, the amplitude of electron transfer to Cu_A after CO dissociation starts to decrease and becomes zero at the fully reduced state of the enzyme.

Interestingly, at high pH, electron backflow is also supplemented by a millisecond phase ($\tau \sim 2$ msec, pH 9) caused by

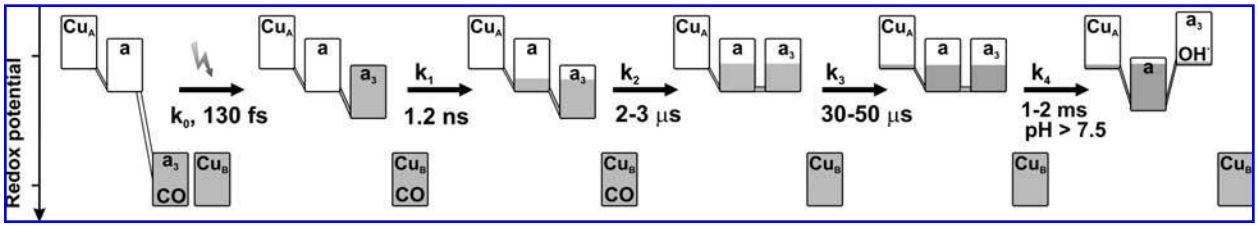

FIG. 10. The scheme of the electron backflow reaction from the mixed-valence CcO. Each box represents one of the redox centers and can be completely or partially filled (reduced), or emptied (oxidized). During the backflow reaction, an electron from heme a_3 sequentially travels from heme a_3 to heme *a* and Cu_A. At the end of the reaction, the electron is equilibrated among all redox centers with respect to their redox potential. At alkaline pH, the backflow reaction is supplemented with an additional phase because of proton release from a water molecule in the vicinity of heme a_3.

proton release (6, 79) from the enzyme *via* the K pathway to the bulk solution with concurrent electron equilibration between redox centers. In this process, a molecule of water at the active site forms a hydroxide anion that binds to the ferric heme a_3 (25, 37). Noteworthy, the rate of proton release from the enzyme strongly depends on the surrounding of the protein. In soluble CcO, the rate is ~1–2 msec; however, when the enzyme is reconstituted into phospholipid vesicles, the proton ejection rate becomes ~10-fold faster, at 150 μsec (25). Two possible explanations for this effect are as follows:

1. either reconstitution of CcO into the vesicles changes the conductivity of the K channel, or
2. the large negatively charged surface of the membrane attracts the proton, increasing the rate of its release.

Thus, the electron redistribution in the mixed-valence enzyme after CO photolysis can be described as a cascade of equilibrium events shown in Fig. 10. First, on the time scale of 1 nsec, the electron reequilibrates between the hemes, and most likely, this equilibrium includes Cu_B, because all three centers are located close enough to enable fast electron transfer. During the next 3-μsec step, additional electron redistribution between the same players occurs, probably because of release of CO from Cu_B. The third event with a characteristic time of ~30 μsec appends Cu_A into this quasi-equilibrium system, resulting in participation of all four redox centers in electron reequilibration. At alkaline pH, the system adds one more wave of reequilibration connected to the dissociation of the proton from the water molecule located at the catalytic site in the vicinity of heme a_3. During this process, OH^- binds to the oxidized high-spin heme and, in this way, reduces its redox potential. The latter induces additional electron reequilibration between all redox centers on the time scale of 1 msec for the soluble or 100 μsed for membrane-bound enzyme.

VIII. INTERACTION OF TERMINAL OXIDASES WITH OXYGEN

A. Oxygen trapping by terminal oxidases

The apparent affinity of mitochondrial CcO for oxygen is adjusted by evolution to the content of oxygen in the human tissues. The measured value for the apparent K_m for the CcO from heart muscle mitochondria is ~0.4 μM (75). However, the real dissociation constant obtained from the measurements of oxy-complex formation rates at different oxygen concentrations is ~300 μM (55, 241). This is very weak affinity because, for example, even air-saturated water (258 μM oxygen) does not contain enough oxygen to provide half-saturation of the enzyme. How then is the enzyme capable of a very good apparent affinity for oxygen in tissues, while having such a bad oxygen-binding constant? The increase of oxygen affinity for heme a_3 can be easy realized by raising its midpoint redox potential for the oxygen-bound state, or in other words, by expending some of the redox energy for oxygen binding. However, the respiratory chain in mitochondria evolves to produce $\Delta\mu H^+$ with the maximal efficiency. That is why, most likely, another way was selected during evolution to solve this problem.

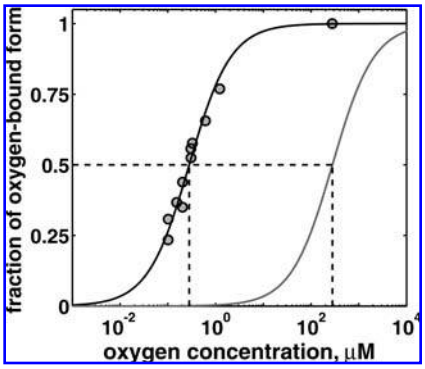

FIG. 11. Comparison of oxygen binding to high-affinity cytochrome *bd* and to cytochrome *c* oxidase. Cytochrome *bd* from *Escherichia coli* has a strong oxygen-binding constant (~280 n*M*), whereas for cytochrome *c* oxidase, this constant is about three orders of magnitude weaker (~280 μM).

The bimolecular rate constant of oxygen interaction with the enzyme is high enough [$1.38 \times 10^8\ M^{-1}\text{sec}^{-1}$ for CcO (241)] to achieve binding of an oxygen molecule to the enzyme active site every 2 msec at the average oxygen concentration in tissues [3 μM (75)]. At the same time, because of the very weak binding constant, the bound oxygen molecule will escape from the binuclear center in 25 μsec ($k_{off} = K_d \times k_{on} = 4.2 \times 10^4$/sec). The only way to work efficiently under such conditions is kinetically to trap oxygen (*i.e.,* to initiate its reduction faster or at least on the same time scale as its escape rate). The experiments showed that the rate constant of transformation of compound **A** into the "peroxy" state is approximately similar to the k_{off} value (see later). This means that CcO has a kinetically effective trap for oxygen (55, 237), in which the molecule of bound dioxygen is rapidly reduced, before it can dissociate.

In contrast, nonpumping cytochrome *bd*–type oxidases have significant decrease of excess redox energy from ubiquinol/quinone to the oxygen/water couple, but this energy is not used for proton pumping across the membrane. Thus, it can be transformed into tight binding of oxygen. The isolation of cytochrome *bd* showed that in "as prepared" state, it exists in the oxygen-bound form, and the removal of oxygen is not an easy task. The determination of the oxygen dissociation constant (24) revealed (Fig. 11) three orders of magnitude difference in the K_d value for pumping heme–copper oxidases in comparison with nonpumping cytochrome *bd*. This difference in oxygen-binding properties corresponds to the increase in the redox potential of the oxygenated heme of 180 mV.

B. Reactive oxygen species and cytochrome c oxidase

Dioxygen is the final acceptor of electrons in the respiratory chain. The role of dioxygen as the main electron sink in living organisms is favored by two main factors: on the one hand, it has high redox potential [$E_m^7(O_2{}^{1\ amt}/2\ H_2O^{55M}) = +820$ mV], which guarantees high energy output from its reduction; and on the other, the reduction of the atmospheric dioxygen has a relatively high activation energy that makes it inert to uncontrolled

reduction. Nevertheless, reactions resulting from the uncontrolled reduction of dioxygen in cells are still present. These reactions lead to generation of the reactive oxygen species (ROS): one-electron reduction to superoxide (O_2^-), two-electron reduction to hydrogen peroxide (H_2O_2), and three-electron reduction yields hydroxyl radical ($OH^{\cdot}$). These ROS are highly reactive and cause nonspecific damage to proteins, DNA, and lipids. The increased level of ROS in cells is also thought to be linked with aging and some degenerative deceases (45, 68, 178). In addition, recent results suggest that the moderate generation of ROS during normal oxygen metabolism is important for cell regulation and signaling (13, 268). The main source of ROS in mammalian cells is the mitochondrial respiratory chain. Interestingly, even though CcO is the only protein in the respiratory chain that directly interacts with oxygen, it is not responsible for ROS production. The primal source of ROS in the respiratory chain is two other proton-translocating complexes—NADH dehydrogenase and bc_1-complex (223, 224). The rate of ROS formation strongly depends on the amplitude of membrane potential: high $\Delta\Psi$ raises the reduction level of the respiratory chain and thus favors ROS generation, whereas decrease of $\Delta\Psi$ leads to decrease of ROS production (89). The overreduction of the respiratory chain occurs also under hypoxic conditions. In this situation, generation of ROS is regulated by two mechanisms. First, the cell metabolism is switched to the anaerobic pathway by inducing expression of lactate dehydrogenase A, which converts pyruvate into lactate, thus reducing formation of NADH; and second, CcO activity is optimized by the expression of different isoforms of regulatory subunits (201).

Absence of ROS production during the catalytic reaction of CcO is due to very fast oxygen activation and reduction when all four electrons required for splitting of the O-O bond are simultaneously delivered to dioxygen without the involvement of any partial oxygen-reduction steps.

IX. INTERMEDIATES OF THE CATALYTIC CYCLE

In contrast to most cell proteins, the redox centers of CcO are colored and characterized by distinct optical spectra in oxidized and reduced states, and mainly because of that, the basic knowledge about intermediates of the catalytic cycle was obtained by optical absorbance spectroscopy. For example, development of the flow-flash reaction, measured by optical absorbance spectroscopy at 584 nm, shows at least five distinct transitions (Fig. 12, solid curve). Furthermore, when the kinetics of optical changes are known for the whole spectral range, it is possible to obtain the spectra of individual intermediates of the cycle. For a deeper understanding of internal processes in the catalytic cycle, the optical studies are often supplemented with other measurements, like determination of potential generation across the membrane (Fig. 12, dashed curve), or measurements of proton uptake and release.

Approximately up to 10 intermediates of the catalytic cycle were identified (Fig. 13); some of them are more or less stable, whereas the others appear only for a fraction of a millisecond. It should be noted that the letter abbreviations accepted in the literature for the different states reflect only the state of the binuclear site and do not specify the redox states of heme *a* and Cu_A.

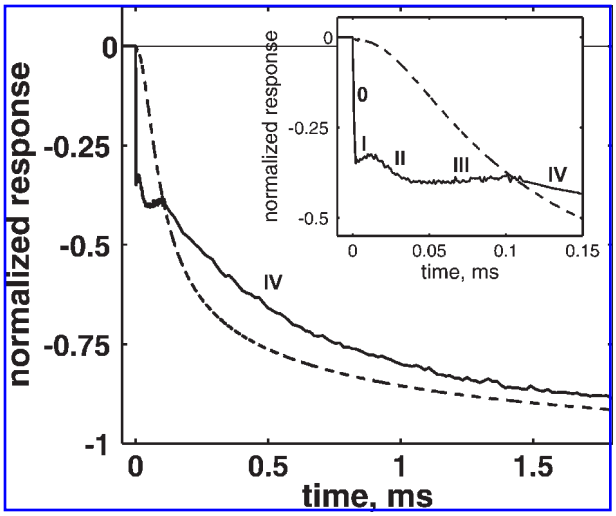

FIGURE 12. Comparison of electrometric (*dashed trace*) and optical (at 584 nm, *solid trace*) time courses for the reaction of CcO with dioxygen (flow-flash reaction) at neutral pH. From the optical trace, it can be seen that the initial phase of CO photolysis (0) is followed by at least four phases (denoted by roman numbers from I to IV) of the catalytic reaction. Roughly, phase I is formation of compound **A**; phase II, $\mathbf{A} \rightarrow \mathbf{P_R}$; phase III, $\mathbf{P_R} \rightarrow \mathbf{F}$; and phase IV, $\mathbf{F} \rightarrow \mathbf{O}$. The inset shows the same curves on a shorter time span.

A. *Fully oxidized **O** state*

The enzyme after purification is in the fully oxidized "as prepared" state, in which all redox centers of the protein are oxidized, and the enzyme cannot react with dioxygen. However, depending on the details of the purification protocol, it may sometimes contain a fraction of an electron and be partially at the **E** (one-electron reduced) state. The enzyme at the **O** state is present in different substates, depending on a ligand bound to the high-spin heme. These substates can roughly be divided into two groups based on their ability to react with cyanide (20, 146). One—the "slow" form—has a maximum in the Soret region of <418 nm and is characterized by slow kinetics of cyanide binding to the oxidized heme a_3. The absorbance maximum of the other "fast" form is several nanometers red-shifted; this form binds cyanide at least 100-fold more rapidly. The enzyme in the slow form can be obtained when the protein is incubated or purified in a low-pH buffer (~6), especially in the presence of certain anions such as Br^-, $HCOO^-$, or Cl^- (20, 146). At the same time, the fully oxidized, as prepared, state is often referred to as the "resting" form of the oxidase, and it can include both slow and fast forms. Reduction and reoxidation (*pulsing*) of the resting oxidase produces the homogeneous population of the oxidized **O** state—the so-called "pulsed" form (12). The pulsed form is highly active and has properties very similar to those of the fast form, although most likely, these forms represent different states of the enzyme discriminated by the ability to pump protons on reduction (23, 33, 235). Thus,

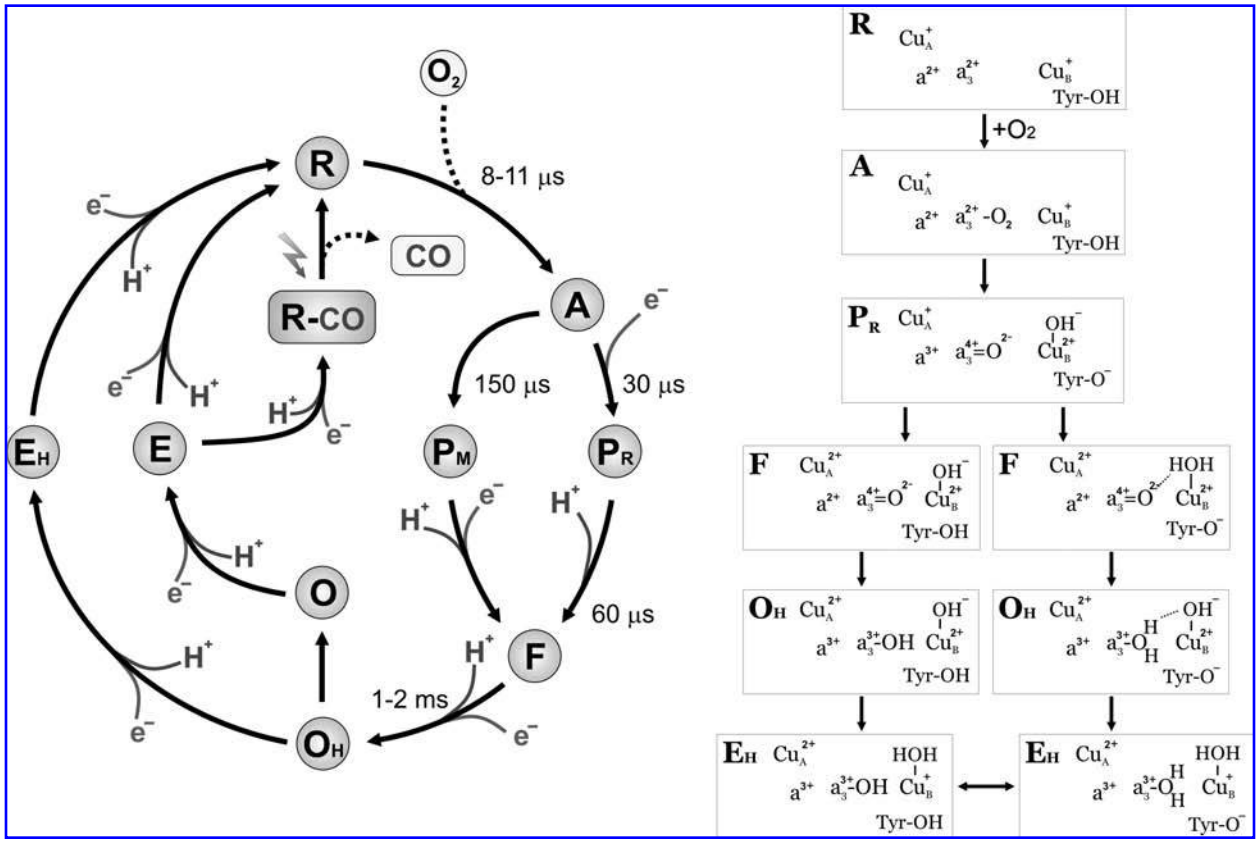

FIG. 13. The catalytic cycle of cytochrome *c* oxidase supplemented by the plausible structures of the intermediates. The definitive structure of the **F** state is still unclear, and two possible configurations may be proposed. The acceptor of a proton during the $\mathbf{P_R} \rightarrow \mathbf{F}$ transition is either tyrosinate or the OH^- ligand of Cu_B. The duality of **F** leads to different possible configurations of the $\mathbf{O_H}$ and $\mathbf{E_H}$ states.

the pulsed form is probably the same state as the $\mathbf{O_H}$ intermediate in the catalytic cycle (see later).

*B. One-electron reduced **E** state*

In the **E** state, an electron is shared between heme a_3 and Cu_B in the binuclear center. This state can be obtained in potentiometric titrations, where it is characterized by the appearance of the g = 6 EPR signal. This signal originates from the oxidized high-spin heme a_3 (when Cu_B is reduced), and the maximal amplitude of the g = 6 EPR signal (257) in the potentiometric redox titration would indicate maximal yield of the **E** state. Alternatively, it is possible to create **E** by several kinetic techniques, such as flash-induced chemical photoreduction (FIRE) (145) or electron injection (155, 194, 244). However, it should be stressed that formation of the **E** state by kinetic techniques takes seconds, because of extremely slow proton uptake to the binuclear center for charge compensation. Taking into account that the complete cycle of CcO occurs in several milliseconds, it is rather unlikely that the **E** state is a natural state during catalytic turnover of the oxidase. Unlike hemoglobin or myoglobin, one-electron reduced CcO cannot bind either oxygen or carbon monoxide.

*C. Reduced **R** state*

The **R** state is the state that is capable of dioxygen binding and can have from two to four electrons in the redox centers. Delivery of an electron alone into low-dielectric media deep in the middle of the membrane, where three of four enzyme redox centers are located, is energetically unfavorable but can be enhanced when coupled to proton uptake. And indeed, Mitchell and Rich (144), based on experimental determination of proton uptake upon reduction and binding of anions (azide, formate, fluoride, or cyanide), suggested an electroneutrality principle, which postulates that reduction of the binuclear center is coupled to uptake of two protons for charge compensation. Complete reduction of the oxidase by four electrons is coupled to uptake of 2.1 to 2.4 H^+/CcO in *R. sphaeroides* and bovine oxidases (4, 51, 144). At least two of these protons are taken up *via* the K pathway and most likely are used for water formation (6, 103, 123, 250). Both fully reduced and mixed-valence (two-electron reduced) oxidases can bind CO to heme a_3. Binding of CO to the binuclear center increases midpoint potentials of heme a_3 and Cu_B, and stabilizes their reduced form (258). Depending on the reduction level of the oxidase, two types of CO-bound compounds are defined: the fully reduced CO-bound

(*COFR*) form with all four redox centers in the reduced state, and the mixed-valence CO-bound (*COMV*) form, in which only a_3 and Cu_B are reduced. Both forms, COFR and COMV, are widely used as a starting point for studies of intermediates in the reaction cycle.

*D. Ferrous-oxy **A** intermediate*

As mentioned in the previous paragraph, the oxidase already in the two-electron reduced state can rapidly react with dioxygen, producing the so-called compound **A**. Compound **A** is the first spectroscopically detectable intermediate originally reported by Chance *et al.* (55) in their low-temperature "triple-trapping" experiments with a 591-nm peak and 611-nm trough in the difference spectrum. At room temperature, compound **A** is formed with a time constant of 8 μsec at 1 m*M* oxygen concentration (157, 241) and has an absorbance maximum at 595 nm (92, 214, 238). Similar to oxyhemoglobin and oxymyoglobin, the Raman spectrum of compound **A** (84, 230) has a stretching mode at 568 per cm, which characterizes the $Fe_{a3}{}^{2+}$-O_2 structure of the binuclear center.

E. Peroxy intermediate, P_M

Compound **A** is unstable and, in the case of the mixed-valence enzyme, decays with $\tau \sim 150$ μsec (92, 157) into the so-called peroxy ($\mathbf{P_M}$) intermediate, originally named compound C (55). Subscripts $_{\cdot M'}/_{\cdot R}$ in **P** were introduced in (151) to distinguish the origins of two peroxy-oxygen intermediate forms—mixed-valence and fully reduced, respectively. The $\mathbf{P_M}$ intermediate is stable, and the reaction stops here unless an additional electron enters the enzyme. This compound was named "peroxy" because it was thought that the oxygen–oxygen bond is still intact in it, and heme a_3 has a peroxy structure $Fe_{a3}{}^{3+}$-O^-O^-. But more recent examination by kinetic resonance Raman (172), and mass-spectrometry (64) clearly demonstrated that the oxygen–oxygen bond is already broken, and heme a_3 is in the oxo-ferryl state ($Fe_{a3}{}^{4+}$ = O), with another oxygen atom being bound to Cu_B as a hydroxide ion. The $\mathbf{P_M}$ state can also be formed directly in the reaction of the oxidized CcO at alkaline pH with stoichiometric amounts of H_2O_2 (29, 245, 262), in which the resulting spectrum has characteristic peaks at 607 (ε_{607}–$\varepsilon_{630} \sim 11$ mM^{-1}cm^{-1}) and 570 nm in the $\mathbf{P_M}$-*minus*-**O** difference spectrum. Cleavage of the O-O bond requires simultaneous transfer of four electrons to the molecule of dioxygen. Three of these electrons are donated from the metals of the binuclear center: one from Cu_B ($Cu_B{}^+ \rightarrow Cu_B{}^{2+}$) and two from the heme a_3 iron ($Fe_{a3}{}^{2+} \rightarrow Fe_{a3}{}^{4+}$), although the source of the fourth electron is still under debate. Presumably, the fourth electron is donated from one of the amino acid residues in the proximity of the catalytic site. High-resolution x-ray crystallographic structures (162, 265) and biochemical analysis (43) revealed that conservative $Tyr280_I$(244) in the catalytic center is covalently linked (Fig. 5) to one of the ligands of Cu_B [$His276_I$(240)], and was proposed to serve as a source of the remaining electron. In addition to electron transfer, O-O bond cleavage requires delivery of a proton. Reaction of COMV with oxygen occurs without external proton uptake (158), indicating that the required proton must be borrowed from one of the groups within the oxidase. At the same time, electrometric results show virtually no phase of potential generation during $\mathbf{R} \rightarrow \mathbf{P_M}$ reaction (108); thus, most likely the required proton is taken from a group very close to the catalytic center. Taken together, it is reasonable to propose that $Tyr280_I$ provides both an electron and a proton for O-O bond splitting, producing the neutral tyrosine radical (172, 173).

F. Peroxy intermediate, P_R

When the oxygen reacts with the fully reduced oxidase, compound **A** relaxes into another unstable peroxy intermediate ($\mathbf{P_R}$) in ~30–40 μsec (157, 241). As was shown by the optical absorbance spectroscopy (90, 91) and by resonance Raman examination (83), a significant fraction of heme *a* becomes oxidized on formation of $\mathbf{P_R}$, whereas Cu_A stays reduced (160). At the same time, $\mathbf{P_M}$ and $\mathbf{P_R}$ have very similar kinetic difference spectra, with the only variation due to a heme *a* oxidation in the latter (151, 214), indicating similar structures of the catalytic site with the O-O bond already broken (149) in both these intermediates. However, because of electron transfer from heme *a* in the latter case, the cross-linked tyrosine donates a proton only and turns into deprotonated tyrosinate rather than a radical. As with the formation of $\mathbf{P_M}$, the appearance of $\mathbf{P_R}$ is not coupled to proton uptake from the bulk solution (4, 116), but internal proton movement is very likely to occur (26, 116, 149). $\mathbf{P_R}$ is a unique state in the catalytic cycle, because it is the only state in which electron transfer into the binuclear center is not coupled to external proton uptake and is kinetically distinguishable from the following proton uptake in the next transition. Such a feature of $\mathbf{P_R}$ is most likely due to preceding protonation of some internal sites on formation of COFR, which would favor fast electron transfer.

*G. Ferryl-oxo intermediate **F***

Intermediate **F** can be obtained in several ways: by the reversal of electron transfer when high proton-motive force is applied to mitochondria (247); in the flow-flash reaction from $\mathbf{P_R}$ with $\tau \sim$ 120–140 μsec in bovine CcO (93, 157), or in 50 μsec in CcO from *P. denitrificans* (182); by electron injection into the stable $\mathbf{P_M}$ state (243); or by incubation of oxidized CcO with excessive amounts of H_2O_2 (246, 262). Intermediate **F** can be easily detected by optical absorbance spectroscopy, as it has a characteristic peak at 580 nm in the **F**-*minus*-**O** difference spectrum (ε_{580}–$\varepsilon_{630} \sim 5.3$ mM^{-1}cm^{-1}). From the structural point of view, the difference between **F** and $\mathbf{P_R}$ is an extra proton in the catalytic center in the former intermediate. This proton is taken up from the N-side of the membrane *via* the D pathway (Fig. 9), although the **F** state can also be formed even when the D channel entrance is blocked by mutation (209). In this case, the required proton may be borrowed from one of the amino acid residues forming the channel—presumably $Glu278_I$(242). The exact target of the chemical proton in the $\mathbf{P_R} \rightarrow \mathbf{F}$ transition is uncertain, but two possible candidates can be proposed: in one scenario, this proton binds to Tyr-O^-, whereas in the other, it transforms the hydroxyl group at Cu_B to a water molecule (Fig. 13). Proton uptake to the catalytic center during $\mathbf{P_R} \rightarrow \mathbf{F}$ is

also coupled with $Cu_A \leftrightarrow$ heme *a* electron reequilibration (157), in which ~60% of Cu_A is oxidized (90).

H. Fully oxidized high-energy state, O_H

The $\mathbf{O_H}$ state is a final product in the classic flow-flash reaction of the fully reduced CcO with dioxygen. It appears with a time constant of 1–2 msec (90, 93, 157) from **F** and requires delivery of both an electron and a chemical proton to the catalytic site. While the electron migrates from the Cu_A/heme *a* couple, the proton is taken up *via* the D pathway (123), as in the $\mathbf{P_R} \rightarrow \mathbf{F}$ transition. Most likely, the chemical proton goes to the oxygen atom at the heme a_3 iron, resulting in two possible configurations of the catalytic center: in one case (left branch in scheme, Fig. 13), both heme a_3 and Cu_B have hydroxide ligands, whereas in the other, these two metal centers share water and hydroxide molecules. In the latter case, the hydroxide ion and the water molecule form a resonance structure with a preferable configuration in which the water molecule is bound to the heme a_3 iron and the hydroxide to Cu_B. The fully oxidized $\mathbf{O_H}$ state is referred to as a "high-energy" state, implying that the energy released in the redox reactions of the oxidative part of the catalytic cycle is conserved in this intermediate (235) and will be used during the next transitions of the cycle for proton pumping (23, 33). The $\mathbf{O_H}$ state is not stable, and in certain conditions, when the electron donors are exhausted, it relaxes into the low-energy **O** state (incapable of pumping protons on reduction) possibly by a protonation of a hydroxyl to water, or tyrosinate to tyrosine. Despite the energetic difference, no spectral distinction between **O** and $\mathbf{O_H}$ intermediates was found (106).

I. One-electron reduced E_H

Discovery of the metastable high-energy $\mathbf{O_H}$ state had led to the conclusion that its reduction will result in formation of a one-electron reduced state, which will be different from the relaxed **E** created by the reduction of the resting CcO (23, 33). Not much is yet known about the structure of this intermediate; however, recent results already indicate that the Cu_B center receives an electron on the $\mathbf{O_H} \rightarrow \mathbf{E_H}$ transition ($Cu_B^{2+} \rightarrow Cu_B^{+}$), with a chemical proton being delivered to the catalytic center (23).

X. PROTON PUMPING

From the discovery of cytochromes by David Keilin in the 1920s (117, 118), it took >40 years of investigation (208) to find that CcO maintains $\Delta\mu_H^+$ on a membrane by vectorial organization of chemistry, and 10 more years to prove that for maximal efficiency, the enzyme can perform an active transport of protons from one side of the membrane dielectric to the other (*pumping*). As was first shown by Wikström (255) with rat-liver mitochondria and confirmed later with bovine CcO reconstituted in phospholipid vesicles (53, 124, 256), reduction of each dioxygen to two molecules of water is coupled to pumping of four protons from the N- to the P-side of the membrane.

A. Stoichiometry of proton translocation in the catalytic cycle

The first attempts to correlate proton pumping with certain transitions in the catalytic cycle were done by a quasi-equilibrium approach by reversal of the oxygen reduction reaction. The application of high electrochemical proton gradient across the inner mitochondrial membrane with high E_h and relatively high pH of the medium creates specific conditions in which some catalytic steps of dioxygen reduction could be reversed. Thus, addition of a high concentration of ATP to well-coupled mitochondria leads to the formation of **F** from **O**; the following increase in the redox potential drives the conversion of **F** into **P** (247, 252). Analysis of the yields of the **F** and **P** intermediates from the applied driving force at different pH values (249) led to the conclusion that the four-electron transfer steps in the catalytic cycle are not equal with respect to proton pumping, and all four protons are pumped in two equal parts only during the $\mathbf{P} \rightarrow \mathbf{F}$ and $\mathbf{F} \rightarrow \mathbf{O}$ transitions.

These conclusions were challenged by Michel (138), who reanalyzed the original experiments and proposed a new model. The stoichiometry of the proton pumping predicted by this model was two protons in $\mathbf{P_R} \rightarrow \mathbf{F}$, one in $\mathbf{F} \rightarrow \mathbf{O}$, and one more proton in the reductive part of the cycle, presumably during the **E** to **R** transition.

Detailed analysis of membrane-potential generation combined with parallel optical measurements of the flow-flash reaction showed that both $\mathbf{P_R} \rightarrow \mathbf{F}$ or $\mathbf{P_M} \rightarrow \mathbf{F}$, and $\mathbf{F} \rightarrow \mathbf{O}$ transitions generate approximately equal amounts of potential (107, 108, 239). However, despite an extremely good signal-to-noise ratio for the electrometric signals, this method does not directly give the number of transferred charges. One solution to this problem is to use an internal standard for the calibration. Such independent calibration of potential generation can be obtained, for example, from the electron-backflow reaction (see later), which at neutral pH consists of a single electrogenic event: electron transfer from heme *a* to Cu_A. But even in the backflow case, such calibration is complicated by uncertainty in the dielectric distance between these redox centers [*i.e.,* how deeply heme *a* is buried in a membrane (108)]. The x-ray crystallographic structure of the oxidase (105, 220) and experimental determination (25, 235) of the dielectric depth gave the value of one third, implying that the pumping stoichiometry is one in both the $\mathbf{P} \rightarrow \mathbf{F}$ and $\mathbf{F} \rightarrow \mathbf{O}$ transitions.

Direct measurements of both proton and charge translocations in CcO vesicles during partial turnover of the enzyme (33, 235) showed that actually only two protons are pumped in the oxidative part of the catalytic cycle: one during $\mathbf{P} \rightarrow \mathbf{F}$, and another during $\mathbf{F} \rightarrow \mathbf{O}$, which, however, is supplemented by two more protons when the oxidation is followed by immediate re-reduction. Because reduction of the fully oxidized **O** state is not coupled to proton pumping (33, 194, 235, 244), a new "high-energy" fully oxidized $\mathbf{O_H}$ intermediate with energy conserved for proton translocation was proposed. Indeed, by electron-injection experiments, it was proved that one-electron reduction of $\mathbf{O_H}$ leads to formation of a new $\mathbf{E_H}$ state and coupled with translocation of one proton across the membrane (23, 33). Because the overall stoichiometry of proton translocation is four protons per dioxygen, reduction of the $\mathbf{E_H}$ state should also be coupled to

proton translocation, and indeed, electron-injection experiments confirm this assignment (33, 193).

The results of all these experiments have been developed into a symmetrical scheme of the pumping events during the catalytic cycle of CcO (Fig. 14). Under continuous-turnover conditions, CcO proceeds *via* four relatively stable intermediates: $\mathbf{P_M}$, **F**, $\mathbf{O_H}$, and $\mathbf{E_H}$. Single-electron reduction of each of these four intermediates from cytochrome *c* leads to uptake of a chemical proton from the N-side with simultaneous translocation of a pumped proton across the membrane.

B. Thirty years of proton-pump modeling

It was always assumed that proton pumping is coupled with the reduction and oxidation of certain redox centers of CcO, and at different times, each of the four redox centers was considered to be a crucial element in the mechanism of proton translocation.

The model of ligand exchange at the Cu_A site due to its oxidoreduction was proposed by the Chan group (71). In this model, reduction of Cu_A induces a change of the Cu_A ligand state, which results in proton translocation from a tyrosine residue below Cu_A to one of the cysteine ligands of Cu_A. On further oxidation of Cu_A by the binuclear center, the composition of the system returns to its original configuration with release of the translocated proton from the cysteine and reprotonation of the tyrosine residues. However, this model seems to be unfeasible because structurally similar quinol oxidases are still able to pump protons, even in the absence of a Cu_A center.

Heme *a* was probably the most popular candidate for being a key redox center for proton pumping. For more than 20 years after discovery of proton pumping, the idea of tight coupling of heme *a* oxidoreduction to proton pumping was used in many models (15, 16, 138, 164, 184, 253, 265). In general, it was proposed that reduction of heme *a* is coupled to uptake of a pumped proton from the N-side of the membrane. Subsequent electron transfer from heme *a* to the binuclear center is linked to uptake of another proton from the N-side for water formation, and release of the preloaded proton toward the P-side of the membrane.

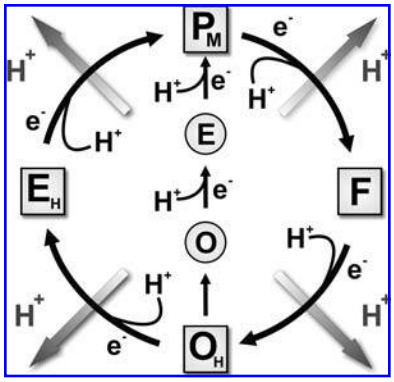

FIG. 14. Proton-pumping steps during the catalytic cycle of cytochrome *c* oxidase. The active states are shown in *squares*. Each transition between them is coupled to proton pumping. The relaxed states are shown in *circles*. Their reduction is not coupled to proton pumping.

Rousseau *et al.* (192) proposed a model in which oxidoreduction of heme a_3 is linked to change of its ligand configuration: in one redox state, a histidine residue occupies the fifth coordination site of the heme, whereas in another, the histidine is substituted by a tyrosine. Such exchange leads to proton translocation from the tyrosine to histidine and further to the P-side of the membrane.

Several models have put oxidoreduction of Cu_B as a central element in the proton-translocation mechanism. Mitchell (142) proposed that reduction of Cu_B leads to protonation from the N-side of its hydroxyl ligand to water, with the following redirection of the water molecule toward the P-side, after which, the proton is released due to Cu_B oxidation. Another model (129) that posits Cu_B as a central element in the proton pump is derived from Chan's Cu_A model of ligand exchange. A "histidine cycle" model presented in 1994 (150) specifies one of the conserved histidine ligands of Cu_B as a pump element. According to this model, this histidine can shuttle between two conformations, depending on the reduction level of Cu_B. In one conformation, the histidine is deprotonated (imidazolate form, Im^-) and bound to Cu_B, whereas in another form, it is protonated (imidazolium, $ImHH^+$) and rotated away from Cu_B. Arrival of a chemical proton to oxygen induces proton ejection from the imidazolium toward the P-side of the membrane and serves as a driving force for the reaction.

In contrast, recent models do not posit a single redox cofactor as a driving element of proton translocation but rather one of two processes: a transfer of an electron from heme *a* to the binuclear center (171, 206, 207), which is then followed by proton delivery to the pump site above the hemes; or a transfer of a proton from the conserved $Glu278_I$(242) to the proton-pump site, which triggers electron equilibration between the hemes (23, 26, 254). Despite their different postulations regarding the driving reaction step of proton translocation, these models are quite similar. The first step of electron (heme *a* to the binuclear center) and proton (from $Glu278_I$ to the pump site) translocation is followed by uptake of a chemical proton to the active site, which leads to release of the pumped proton out of the protein at the P-side.

A model that is completely different from the just-described electrostatic models was recently proposed by the Brzezinski group. Based on the kinetics of proton uptake and release on both aqueous sides of the membrane, it was suggested that proton pumping is not coupled to internal electron transfer, but rather occurs as a result of energy conservation in the protein structure in response to transfer of a chemical proton to the active site (42, 66).

So the long history of CcO studies has produced a large number of models to explain the proton-pump mechanism; many of these models have already been disproved, but we should admit that still no single widely accepted theory exists.

C. Single-proton translocation cycle

In the continuous-turnover regimen, the catalytic cycle of CcO consists of four proton-translocation steps (Fig. 14). During each step, delivery of an electron to the enzyme starts a proton-pump cycle, which is likely to occur by essentially the same

mechanism every time the electron arrives. In principle, the mechanism of proton translocation during a single pump event can be studied at any of these steps; however, the $\mathbf{O_H \rightarrow E_H}$ transition is preferable because of high yield (almost 100%) of the $\mathbf{O_H}$ state formation in the reaction of the fully reduced CcO with dioxygen. The $\mathbf{O_H \rightarrow E_H}$ reaction can be initiated by electron injection from the photosensitive dye RubiPy and followed by both time-resolved optical spectroscopy and electrometry. Correlation of results from both these techniques allowed the construction of a comprehensive scheme to portray a single proton-translocation cycle during catalytic turnover (26).

During single-electron reduction of the $\mathbf{O_H}$ state of CcO, the electron first enters the Cu_A center. In the next phase, the electron equilibrates between Cu_A and heme *a*, with $\tau \sim 10$ μsec (Fig. 15, I $\rightarrow$ II transition). In this phase, ~70% of the electron is transferred from Cu_A to heme *a*. Because the midpoint redox potential (E_m) of Cu_A is 250 mV (76, 271), it is possible to estimate the E_m value for heme *a* as ~270 mV. Absence of electron transfer to the binuclear center during the 10-μsec phase indicates that the E_m values of heme a_3 and Cu_B must be at least 120 mV lower than that of heme *a*. Electron equilibration between Cu_A and heme *a* is not coupled to proton uptake (157, 194, 207), resulting in the relatively low "operational" E_m of heme *a*, which is much lower than the "high asymptotic" E_m found in equilibrium redox titrations (15, 31, 76, 147, 251). However, it is still high enough to take an electron from Cu_A without charge compensation by a proton.

The arrival of an electron to heme *a* increases the pK_a of a yet unidentified "pump site" above the heme groups, which takes up a proton with $\tau \sim 150$ μsec (Fig. 15, II $\rightarrow$ III transition). The protonation of the "pump site" occurs from the conserved $Glu278_I$(242) *via* a chain of water molecules by the Grotthuss mechanism (7, 57, 254) (Fig. 8). Three to four water molecules are predicted inside the hydrophobic cavity between the glutamate, the Δ-propionate of heme a_3, and the binuclear center (187, 270). These water molecules can feel the redox-state–dependent electric field between heme *a* and the binuclear center, and arrange themselves into two different configurations for proton transfer (254). When the binuclear center is oxidized and the electron is on heme *a*, the array of water molecules is oriented toward the Δ-propionate of heme a_3 ("pump site" direction); however, it switches toward the binuclear center (direction for chemical reaction) after reduction of the binuclear center from heme *a*. The rate-limiting protonation of the "pump site" increases the E_m of both hemes, and leads to further electron equilibration between Cu_A and the hemes in the same time window (Fig. 15, III $\rightarrow$ IV transition). At the end of the 150-μsec phase, Cu_A becomes fully oxidized, whereas heme *a* and heme a_3 have 40% and 60% of the injected electrons, respectively. In addition, the 150-μsec phase includes reprotonation of $Glu278_I$ from the N-side of the membrane *via* the D proton–conducting pathway.

In the next phase ($\tau \sim 800$ μsec), transfer of a substrate proton to the OH^- ligand of Cu_B (65) increases the E_m of Cu_B to a value much higher than that for all other redox centers, which induces ultimate movement of the injected electron to the Cu_B center (Fig. 15, IV $\rightarrow$ V transition).

During the last step ($\tau \sim 2.6$ msec) of the single proton-pump cycle, the proton that has been "preloaded" to the pump site is expelled toward the P-side of the membrane because of electrostatic repulsion from the substrate proton.

It seems feasible that the mechanism of proton translocation during $\mathbf{P_M \rightarrow F}$, $\mathbf{F \rightarrow O_H}$, and $\mathbf{E_H \rightarrow R}$ is essentially the same as in the $\mathbf{O_H \rightarrow E_H}$ transition, with the only variation in the final destination of the injected electron. After oxygen activation, CcO has four high-potential acceptors that are sequentially filled with electrons during each of the pumping transition steps. Thus, the sequence of events shown in Fig. 15 would be repeated every time an electron enters the Cu_A site. In each case, an electron travels from cytochrome *c* to Cu_A, and further through heme *a* to the binuclear center, driving proton pumping across the membrane.

ACKNOWLEDGMENTS

The authors' work was supported by grants from Biocentrum Helsinki, the Sigrid Juselius Foundation, and the Academy of Finland. Part of this work represents the Ph.D. thesis of co-author I. Belevich.

ABBREVIATIONS

A, ferrous-oxy intermediate; CCD, charge-coupled device, an image sensor consisting of a large number of photodiodes for light registration; CcO, cytochrome *c* oxidase; COFR, CO-bound fully reduced form of the enzyme; COMV, CO-bound mixed-valence state of the enzyme; **E**, one-electron re-

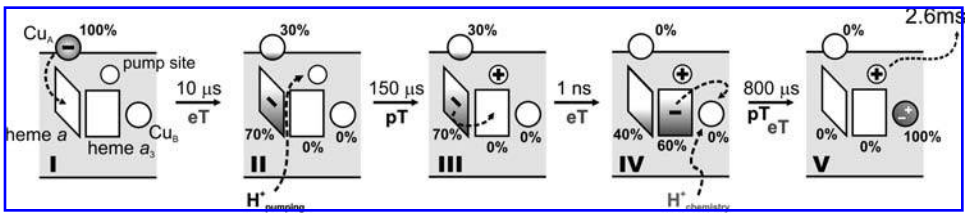

FIG. 15. The scheme of a single proton translocation cycle of cytochrome *c* oxidase. The *rhombus* and *square* represent heme *a*, and heme a_3, respectively; the *circle* above the rhombus represents Cu_A; the circle above the square is a "pump site"; the circle next to the *square* is Cu_B. The *minus sign* denotes where most of the injected electron is positioned. The *percentage numbers* next to the redox centers show the level of electron occupancy of the corresponding center. *Dashed arrows* indicate electron (eT) and proton (pT) transfers during the next reaction step.

duced state; EDTA, ethylenediaminetetraacetic acid; EGTA, ethyleneglycol-bis-(β-aminoethyl either)*N*,*N'*-tetra-acetic acid; $\mathbf{E_H}$, high energy one-electron reduced state; E_h, reduction potential of the medium; E_m, midpoint redox potential relative to the standard hydrogen electrode; EPR, electron paramagnetic resonance; **F**, ferryl-oxo intermediate; K_d, binding constant, as k_{off}/k_{on}; K_m, Michaelis–Menten constant; **O**, fully oxidized, as prepared state; $\mathbf{O_H}$, fully oxidized high-energy state; $\mathbf{P_M}$, "peroxy" intermediate obtained from mixed-valence enzyme; $\mathbf{P_R}$, "peroxy" intermediate obtained from fully reduced enzyme; **R**, state with fully reduced binuclear site; ROS, reactive oxygen species; RubiPy, tris(2,2'-bipyridyl) ruthenium; $\Delta\mu_H{}^+$, electrochemical transmembrane gradient of protons across the membrane; $\Delta\Psi$, amplitude of the electric potential.

REFERENCES

1. Aasa R, Albracht PJ, Falk KE. EPR signals from cytochrome *c* oxidase. *Biochim Biophys Acta* 422: 260–272, 1976.
2. Abramson J, Riistama S, Larsson G, Jasaitis A, Svensson-Ek M, Laakkonen L, Puustinen A, Iwata S, and Wikström M. The structure of the ubiquinol oxidase from *Escherichia coli* and its ubiquinone binding site. *Nat Struct Biol* 7: 910–917, 2000.
3. Ädelroth P, Brzezinski P, and Malmström BG. Internal electron transfer in cytochrome *c* oxidase from *Rhodobacter sphaeroides*. *Biochemistry* 34: 2844–2849, 1995.
4. Ädelroth P, Ek M, and Brzezinski P. Factors determining electron-transfer rates in cytochrome *c* oxidase: investigation of the oxygen reaction in the *R. sphaeroides* enzyme. *Biochim Biophys Acta* 1367: 107–117, 1998.
5. Ädelroth P, Ek MS, Mitchell DM, Gennis RB, and Brzezinski P. Glutamate 286 in cytochrome aa_3 from *Rhodobacter sphaeroides* is involved in proton uptake during the reaction of the fully-reduced enzyme with dioxygen. *Biochemistry* 36: 13824–13829, 1997.
6. Ädelroth P, Gennis RB, and Brzezinski P. Role of the pathway through K(I-362) in proton transfer in cytochrome *c* oxidase from *R. sphaeroides*. *Biochemistry* 37: 2470–2476, 1998.
7. Agmon N. The Grotthuss mechanism. *Chem Phys Lett* 244: 456–462, 1995.
8. Alben JO, Moh PP, Fiamingo FG, and Altschuld RA. Cytochrome oxidase (a_3) heme and copper observed by low-temperature Fourier transform infrared spectroscopy of the CO complex. *Proc Natl Acad Sci U S A* 78: 234–237, 1981.
9. Anraku Y and Gennis RB. The aerobic respiratory chain of *Escherichia coli*. *Trends Biochem Sci* 12: 262–266, 1987.
10. Antalis TM and Palmer G. Kinetic characterization of the interaction between cytochrome oxidase and cytochrome *c*. *J Biol Chem* 257: 6194–6206, 1982.
11. Antholine WE, Kastrau DH, Steffens GC, Buse G, Zumft WG, and Kroneck PM. A comparative EPR investigation of the multicopper proteins nitrous-oxide reductase and cytochrome *c* oxidase. *Eur J Biochem* 209: 875–881, 1992.
12. Antonini E, Brunori M, Colosimo A, Greenwood C, and Wilson MT. Oxygen "pulsed" cytochrome *c* oxidase: functional properties and catalytic relevance. *Proc Natl Acad Sci U S A* 74: 3128–3132, 1977.
13. Apel K and Hirt H. Reactive oxygen species: metabolism, oxidative stress, and signal transduction. *Annu Rev Plant Biol* 55: 373–399, 2004.
14. Arnold S, Goglia F, and Kadenbach B. 3,5-Diiodothyronine binds to subunit Va of cytochrome *c* oxidase and abolishes the allosteric inhibition of respiration by ATP. *Eur J Biochem* 252: 325–330, 1998.
15. Artzatbanov VY, Konstantinov AA, and Skulachev VP. Involvement of intramitochondrial protons in redox reactions of cytochrome *a*. *FEBS Lett* 87: 180–185, 1978.
16. Babcock GT and Callahan PM. Redox-linked hydrogen bond strength changes in cytochrome *a*: implications for a cytochrome oxidase proton pump. *Biochemistry* 22: 2314–2319, 1983.
17. Babcock GT, Callahan PM, Ondrias MR, and Salmeen I. Coordination geometries and vibrational properties of cytochromes *a* and a_3 in cytochrome oxidase from Soret excitation Raman spectroscopy. *Biochemistry* 20: 959–966, 1981.
18. Babcock GT, Vickery LE, and Palmer G. Electronic state of heme in cytochrome oxidase, I: Magnetic circular dichroism of the isolated enzyme and its derivatives. *J Biol Chem* 251: 7907–7919, 1976.
19. Babcock GT and Wikström M. Oxygen activation and the conservation of energy in cell respiration. *Nature* 356: 301–309, 1992.
20. Baker GM, Noguchi M, and Palmer G. The reaction of cytochrome oxidase with cyanide: preparation of the rapidly reacting form and its conversion to the slowly reacting form. *J Biol Chem* 262: 595–604, 1987.
21. Beinert H, Hansen RE, and Hartzell CR. Kinetic studies on cytochrome *c* oxidase by combined EPR and reflectance spectroscopy after rapid freezing. *Biochim Biophys Acta* 423: 339–355, 1976.
22. Beinert H, Wharton DC, Griffiths DE, and Sands RH. Properties of copper associated with cytochrome oxidase as studied by paramagnetic resonance spectroscopy. *J Biol Chem* 237: 2337–2354, 1962.
23. Belevich I, Bloch DA, Belevich N, Wikström M, and Verkhovsky MI. Exploring the proton pump mechanism of cytochrome *c* oxidase in real time. *Proc Natl Acad Sci U S A* 104: 2685–2690, 2007.
24. Belevich I, Borisov VB, Konstantinov AA, and Verkhovsky MI. Oxygenated complex of cytochrome *bd* from *Escherichia coli*: stability and photolability. *FEBS Lett* 579: 4567–4570, 2005.
25. Belevich I, Tuukkanen A, Wikström M, and Verkhovsky MI. Proton-coupled electron equilibrium in soluble and membrane-bound cytochrome *c* oxidase from *Paracoccus denitrificans*. *Biochemistry* 45: 4000–4006, 2006.
26. Belevich I, Verkhovsky MI, and Wikström M. Proton-coupled electron transfer drives the proton pump of cytochrome *c* oxidase. *Nature* 440: 829–832, 2006.
27. Berry EA and Trumpower BL. Isolation of ubiquinol oxidase from *Paracoccus denitrificans* and resolution into cytochrome bc_1 and cytochrome *c*-aa_3 complexes. *J Biol Chem* 260: 2458–2467, 1985.
28. Berry S, Schneider D, Vermaas WF, and Rögner M. Electron transport routes in whole cells of *Synechocystis* sp. strain PCC 6803: the role of the cytochrome *bd*-type oxidase. *Biochemistry* 41: 3422–3429, 2002.
29. Bickar D, Bonaventura J, and Bonaventura C. Cytochrome *c* oxidase binding of hydrogen peroxide. *Biochemistry* 21: 2661–2666, 1982.
30. Blackmore RS, Greenwood C, and Gibson QH. Studies of the primary oxygen intermediate in the reaction of fully reduced cytochrome oxidase. *J Biol Chem* 266: 19245–19249, 1991.
31. Blair DF, Ellis WR Jr, Wang H, Gray HB, and Chan SI. Spectroelectrochemical study of cytochrome *c* oxidase: pH and temperature dependences of the cytochrome potentials: characterization of site-site interactions. *J Biol Chem* 261: 11524–11537, 1986.
32. Blair DF, Witt SN, and Chan SI. Mechanism of cytochrome *c* oxidase-catalyzed dioxygen reduction at low-temperatures: evidence for 2 intermediates at the 3-electron level and entropic promotion of the bond-breaking step. *J Am Chem Soc* 107: 7389–7399, 1985.
33. Bloch D, Belevich I, Jasaitis A, Ribacka C, Puustinen A, Verkhovsky MI, and Wikström M. The catalytic cycle of cytochrome *c* oxidase is not the sum of its two halves. *Proc Natl Acad Sci U S A* 101: 529–533, 2004.
34. Boelens R and Wever R. Electron-transfer processes in carboxycytochrome *c* oxidase after photodissociation of cytochrome $a_3{}^{2+}$-CO. *Biochim Biophys Acta* 547: 296–310, 1979.
35. Bogachev AV, Murtazina RA, and Skulachev VP. H^+/e^- stoichiometry for NADH dehydrogenase I and dimethyl sulfoxide reductase in anaerobically grown *Escherichia coli* cells. *J Bacteriol* 178: 6233–6237, 1996.

36. Bränden G, Bränden M, Schmidt B, Mills DA, Ferguson-Miller S, and Brzezinski P. The protonation state of a heme propionate controls electron transfer in cytochrome *c* oxidase. *Biochemistry* 44: 10466–10474, 2005.
37. Bränden M, Namslauer A, Hansson O, Aasa R, and Brzezinski P. Water-hydroxide exchange reactions at the catalytic site of heme-copper oxidases. *Biochemistry* 42: 13178–13184, 2003.
38. Bränden M, Sigurdson H, Namslauer A, Gennis RB, Ädelroth P, and Brzezinski P. On the role of the K-proton transfer pathway in cytochrome *c* oxidase. *Proc Natl Acad Sci U S A* 98: 5013–5018, 2001.
39. Bränden M, Tomson F, Gennis RB, and Brzezinski P. The entry point of the K-proton-transfer pathway in cytochrome *c* oxidase. *Biochemistry* 41: 10794–10798, 2002.
40. Brzezinski P. Internal electron-transfer reactions in cytochrome *c* oxidase. *Biochemistry* 35: 5611–5615, 1996.
41. Brzezinski P. Internal electron-transfer reactions in cytochrome *c* oxidase. *Biochemistry* 35: 5611–5615, 1996.
42. Brzezinski P and Larsson G. Redox-driven proton pumping by heme-copper oxidases. *Biochim Biophys Acta* 1605: 1–13, 2003.
43. Buse G, Soulimane T, Dewor M, Meyer HE, and Blüggel M. Evidence for a copper-coordinated histidine-tyrosine cross-link in the active site of cytochrome oxidase. *Protein Sci* 8: 985–990, 1999.
44. Bushnell GW, Louie GV, and Brayer GD. High-resolution three-dimensional structure of horse heart cytochrome *c*. *J Mol Biol* 214: 585–595, 1990.
45. Cadenas E and Davies KJ. Mitochondrial free radical generation, oxidative stress, and aging. *Free Radic Biol Med* 29: 222–230, 2000.
46. Calhoun MW, Thomas JW, and Gennis RB. The cytochrome oxidase superfamily of redox-driven proton pumps. *Trends Biochem Sci* 19: 325–330, 1994.
47. Callahan PM and Babcock GT. Origin of the cytochrome *a* absorption red shift: a pH-dependent interaction between its heme a formyl and protein in cytochrome oxidase. *Biochemistry* 22: 452–461, 1983.
48. Cao J, Hosler J, Shapleigh J, Revzin A, and Ferguson-Miller S. Cytochrome aa_3 of *Rhodobacter sphaeroides* as a model for mitochondrial cytochrome *c* oxidase: the *coxII*/*coxIII* operon codes for structural and assembly proteins homologous to those in yeast. *J Biol Chem* 267: 24273–24278, 1992.
49. Cao J, Shapleigh J, Gennis R, Revzin A, and Ferguson-Miller S. The gene encoding cytochrome *c* oxidase subunit II from *Rhodobacter sphaeroides:* comparison of the deduced amino acid sequence with sequences of corresponding peptides from other species. *Gene* 101: 133–137, 1991.
50. Capaldi RA. Structure and function of cytochrome *c* oxidase. *Annu Rev Biochem* 59: 569–596, 1990.
51. Capitanio N, Vygodina TV, Capitanio G, Konstantinov AA, Nicholls P, and Papa S. Redox-linked protolytic reactions in soluble cytochrome-*c* oxidase from beef-heart mitochondria: redox Bohr effects. *Biochim Biophys Acta* 1318: 255–265, 1997.
52. Carroll J, Shannon RJ, Fearnley IM, Walker JE, and Hirst J. Definition of the nuclear encoded protein composition of bovine heart mitochondrial complex I. identification of two new subunits. *J Biol Chem* 277: 50311–50317, 2002.
53. Casey RP, Chappell JB, and Azzi A. Limited-turnover studies on proton translocation in reconstituted cytochrome *c* oxidase-containing vesicles. *Biochem J* 182: 149–156, 1979.
54. Caughey WS, Smythe GA, Okeeffe DH, Maskasky JE, and Smith ML. Heme A of cytochrome *c* oxidase; structure and properties: comparisons with heme B, heme-C and heme-S and derivatives. *J Biol Chem* 250: 7602–7622, 1975.
55. Chance B, Saronio C, and Leigh JS. Functional intermediates in reaction of cytochrome oxidase with oxygen. *Proc Natl Acad Sci U S A* 72: 1635–1640, 1975.
56. Crofts AR. The cytochrome bc_1 complex: function in the context of structure. *Annu Rev Physiol* 66: 689–733, 2004.
57. de Grotthuss CJT. Sur la decomposition de l'eau et des corps qu'elle tient en dissolution a l'aide de l'electricite galvanique. *Ann Chim (Paris)* LVIII: 54–74, 1806.
58. Drachev LA, Jasaitis AA, Kaulen AD, Kondrashin AA, Liberman EA, Nemecek IB, Ostroumov SA, Semenov AY, and Skulachev VP. Direct measurement of electric current generation by cytochrome oxidase, H^+-ATPase and bacteriorhodopsin. *Nature* 249: 321–324, 1974.
59. Drachev LA, Kaulen AD, Semenov AY, Severina II, and Skulachev VP. Lipid-impregnated filters as a tool for studying the electric current-generating proteins. *Anal Biochem* 96: 250–262, 1979.
60. Einarsdottir O. Fast reactions of cytochrome oxidase. *Biochim Biophys Acta* 1229: 129–147, 1995.
61. Einarsdottir O, Caughey WS. Bovine heart cytochrome *c* oxidase preparations contain high affinity binding sites for magnesium as well as for zinc, copper, and heme iron. *Biochem Biophys Res Commun* 129: 840–847, 1985.
62. Einarsdottir O, Dyer RB, Lemon DD, Killough PM, Hubig SM, Atherton SJ, Lopez-Garriga JJ, Palmer G, and Woodruff WH. Photodissociation and recombination of carbonmonoxy cytochrome oxidase: dynamics from picoseconds to kiloseconds. *Biochemistry* 32: 12013–12024, 1993.
63. Einarsdottir O, Georgiadis KE, and Sucheta A. Intramolecular electron transfer and conformational changes in cytochrome *c* oxidase. *Biochemistry* 34: 496–508, 1995.
64. Fabian M, Wong WW, Gennis RB, and Palmer G. Mass spectrometric determination of dioxygen bond splitting in the "peroxy" intermediate of cytochrome *c* oxidase. *Proc Natl Acad Sci U S A* 96: 13114–13117, 1999.
65. Fann YC, Ahmed I, Blackburn NJ, Boswell JS, Verkhovskaya ML, Hoffman BM, and Wikström M. Structure of Cu_B in the binuclear heme-copper center of the cytochrome aa_3-type quinol oxidase from *Bacillus subtilis*: an ENDOR and EXAFS study. *Biochemistry* 34: 10245–10255, 1995.
66. Faxen K, Gilderson G, Ädelroth P, and Brzezinski P. A mechanistic principle for proton pumping by cytochrome *c* oxidase. *Nature* 437: 286–289, 2005.
67. Fetter JR, Qian J, Shapleigh J, Thomas JW, Garcia-Horsman A, Schmidt E, Hosler J, Babcock GT, Gennis RB, and Ferguson-Miller S. Possible proton relay pathways in cytochrome *c* oxidase. *Proc Natl Acad Sci U S A* 92: 1604–1608, 1995.
68. Finkel T. Opinion: Radical medicine: treating ageing to cure disease. *Nat Rev Mol Cell Biol* 6: 971–976, 2005.
69. Fuller SD, Darley-Usmar VM, and Capaldi RA. Covalent complex between yeast cytochrome *c* and beef heart cytochrome *c* oxidase which is active in electron transfer. *Biochemistry* 20: 7046–7053, 1981.
70. Garcia-Horsman JA, Barquera B, Rumbley J, Ma J, and Gennis RB. The superfamily of heme-copper respiratory oxidases. *J Bacteriol* 176: 5587–5600, 1994.
71. Gelles J, Blair DF, and Chan SI. The proton-pumping site of cytochrome *c* oxidase: a model of its structure and mechanism. *Biochim Biophys Acta* 853: 205–236, 1986.
72. Geren LM, Beasley JR, Fine BR, Saunders AJ, Hibdon S, Pielak GJ, Durham B, and Millett F. Design of a ruthenium-cytochrome *c* derivative to measure electron transfer to the initial acceptor in cytochrome *c* oxidase. *J Biol Chem* 270: 2466–2472, 1995.
73. Gibson QH and Greenwood C. Reactions of cytochrome oxidase with oxygen and carbon monoxide. *Biochem J* 86: 541–545, 1963.
74. Gibson QH and Greenwood C. The spectra and some properties of cytochrome oxidase components. *J Biol Chem* 239: 586–590, 1964.
75. Gnaiger E. Oxygen conformance of cellular respiration: a perspective of mitochondrial physiology. *Adv Exp Med Biol* 543: 39–55, 2003.
76. Gorbikova EA, Vuorilehto K, Wikström M, and Verkhovsky MI. Redox titration of all electron carriers of cytochrome *c* oxidase by Fourier transform infrared spectroscopy. *Biochemistry* 45: 5641–5649, 2006.
77. Gray HB and Winkler JR. Electron transfer in proteins. *Annu Rev Biochem* 65: 537–561, 1996.
78. Green GN, Lorence RM, and Gennis RB. Specific overproduction and purification of the cytochrome b_{558} component of the cytochrome *d* complex from *Escherichia coli*. *Biochemistry* 25: 2309–2314, 1986.
79. Hallen S, Brzezinski P, and Malmström BG. Internal electron transfer in cytochrome *c* oxidase is coupled to the protonation of

a group close to the bimetallic site. *Biochemistry* 33: 1467–1472, 1994.
80. Haltia T, Finel M, Harms N, Nakari T, Raitio M, Wikström M, and Saraste M. Deletion of the gene for subunit III leads to defective assembly of bacterial cytochrome oxidase. *EMBO J* 8: 3571–3579, 1989.
81. Haltia T, Saraste M, and Wikström M. Subunit III of cytochrome *c* oxidase is not involved in proton translocation: a site-directed mutagenesis study. *EMBO J* 10: 2015–2021, 1991.
82. Haltia T, Semo N, Arrondo JL, Goni FM, and Freire E. Thermodynamic and structural stability of cytochrome *c* oxidase from *Paracoccus denitrificans*. *Biochemistry* 33: 9731–9740, 1994.
83. Han S, Ching YC, and Rousseau DL. Cytochrome *c* oxidase: decay of the primary oxygen intermediate involves direct electron transfer from cytochrome *a*. *Proc Natl Acad Sci U S A* 87: 8408–8412, 1990.
84. Han S, Ching YC, and Rousseau DL. Primary intermediate in the reaction of oxygen with fully reduced cytochrome *c* oxidase. *Proc Natl Acad Sci U S A* 87: 2491–2495, 1990.
85. Harrenga A and Michel H. The cytochrome *c* oxidase from *Paracoccus denitrificans* does not change the metal center ligation upon reduction. *J Biol Chem* 274: 33296–33299, 1999.
86. Hazzard JT, Rong SY, and Tollin G. Ionic strength dependence of the kinetics of electron transfer from bovine mitochondrial cytochrome *c* to bovine cytochrome *c* oxidase. *Biochemistry* 30: 213–222, 1991.
87. Hendler RW, Pardhasaradhi K, Reynafarje B, and Ludwig B. Comparison of energy-transducing capabilities of the two- and three-subunit cytochromes aa_3 from *Paracoccus denitrificans* and the 13-subunit beef heart enzyme. *Biophys J* 60: 415–423, 1991.
88. Hendriks JH, Jasaitis A, Saraste M, and Verkhovsky MI. Proton and electron pathways in the bacterial nitric oxide reductase. *Biochemistry* 41: 2331–2340, 2002.
89. Herrero A and Barja G. ADP-regulation of mitochondrial free radical production is different with complex I- or complex II-linked substrates: implications for the exercise paradox and brain hypermetabolism. *J Bioenerg Biomembr* 29: 241–249, 1997.
90. Hill BC. The reaction of the electrostatic cytochrome *c*-cytochrome oxidase complex with oxygen. *J Biol Chem* 266: 2219–2226, 1991.
91. Hill BC. Modeling the sequence of electron transfer reactions in the single turnover of reduced, mammalian cytochrome *c* oxidase with oxygen. *J Biol Chem* 269: 2419–2425, 1994.
92. Hill BC and Greenwood C. Spectroscopic evidence for the participation of compound A (Fe_{a3}^{2+}-O_2) in the reaction of mixed-valence cytochrome *c* oxidase with oxygen at room temperature. *Biochem J* 215: 659–667, 1983.
93. Hill BC and Greenwood C. The reaction of fully reduced cytochrome *c* oxidase with oxygen studied by flow-flash spectrophotometry at room temperature: evidence for new pathways of electron transfer. *Biochem J* 218: 913–921, 1984.
94. Hill S, Viollet S, Smith AT, and Anthony C. Roles for enteric *d*-type cytochrome oxidase in N_2 fixation and microaerobiosis. *J Bacteriol* 172: 2071–2078, 1990.
95. Hinchliffe P and Sazanov LA. Organization of iron-sulfur clusters in respiratory complex I. *Science* 309: 771–774, 2005.
96. Hinkle PC. Proton translocation by cytochrome *c* oxidase incorporated into phospholipid vesicles. *Methods Enzymol* 55: 748–751, 1979.
97. Hirst J. Energy transduction by respiratory complex I: an evaluation of current knowledge. *Biochem Soc Trans* 33: 525–529, 2005.
98. Hofacker I and Schulten K. Oxygen and proton pathways in cytochrome *c* oxidase. *Proteins* 30: 100–107, 1998.
99. Horie S and Morrison M. Cytochrome *c* oxidase components. I: purification and properties. *J Biol Chem* 238: 1855–1860, 1963.
100. Horsefield R, Iwata S, and Byrne B. Complex II from a structural perspective. *Curr Protein Pept Sci* 5: 107–118, 2004.
101. Hosler JP, Espe MP, Zhen Y, Babcock GT, and Ferguson-Miller S. Analysis of site-directed mutants locates a non-redox-active metal near the active site of cytochrome *c* oxidase of *Rhodobacter sphaeroides*. *Biochemistry* 34: 7586–7592, 1995.
102. Hosler JP, Ferguson-Miller S, Calhoun MW, Thomas JW, Hill J, Lemieux L, Ma J, Georgiou C, Fetter J, Shapleigh J, Tecklenburg MMJ, Babcock GT, and Gennis RB. Insight into the active-site structure and function of cytochrome oxidase by analysis of site-directed mutants of bacterial cytochrome aa_3 and cytochrome *bo*. *J Bioenerg Biomembr* 25: 121–136, 1993.
103. Hosler JP, Shapleigh JP, Mitchell DM, Kim Y, Pressler MA, Georgiou C, Babcock GT, Alben JO, Ferguson-Miller S, and Gennis RB. Polar residues in helix VIII of subunit I of cytochrome *c* oxidase influence the activity and the structure of the active site. *Biochemistry* 35: 10776–10783, 1996.
104. Hunsicker-Wang LM, Pacoma RL, Chen Y, Fee JA, and Stout CD. A novel cryoprotection scheme for enhancing the diffraction of crystals of recombinant cytochrome ba_3 oxidase from *Thermus thermophilus*. *Acta Crystallogr D Biol Crystallogr* 61: 340–343, 2005.
105. Iwata S, Ostermeier C, Ludwig B, and Michel H. Structure at 2.8 Å resolution of cytochrome *c* oxidase from *Paracoccus denitrificans*. *Nature* 376: 660–669, 1995.
106. Jancura D, Berka V, Antalik M, Bagelova J, Gennis RB, Palmer G, and Fabian M. Spectral and kinetic equivalence of oxidized cytochrome *c* oxidase as isolated and "activated" by reoxidation. *J Biol Chem* 281: 30319–30325, 2006.
107. Jasaitis A, Backgren C, Morgan JE, Puustinen A, Verkhovsky MI, and Wikström M. Electron and proton transfer in the arginine-54-methionine mutant of cytochrome *c* oxidase from *Paracoccus denitrificans*. *Biochemistry* 40: 5269–5274, 2001.
108. Jasaitis A, Verkhovsky MI, Morgan JE, Verkhovskaya ML, and Wikström M. Assignment and charge translocation stoichiometries of the major electrogenic phases in the reaction of cytochrome *c* oxidase with dioxygen. *Biochemistry* 38: 2697–2706, 1999.
109. Joseph-Horne T, Hollomon DW, and Wood PM. Fungal respiration: a fusion of standard and alternative components. *Biochim Biophys Acta* 1504: 179–195, 2001.
110. Kadenbach B, Huttemann M, Arnold S, Lee I, and Bender E. Mitochondrial energy metabolism is regulated via nuclear-coded subunits of cytochrome *c* oxidase. *Free Radic Biol Med* 29: 211–221, 2000.
111. Kadenbach B and Merle P. On the function of multiple subunits of cytochrome *c* oxidase from higher eukaryotes. *FEBS Lett* 135: 1–11, 1981.
112. Kannt A, Lancaster CR, and Michel H. The role of electrostatic interactions for cytochrome *c* oxidase function. *J Bioenerg Biomembr* 30: 81–87, 1998.
113. Kannt A, Pfitzner U, Ruitenberg M, Hellwig P, Ludwig B, Mäntele W, Fendler K, and Michel H. Mutation of Arg-54 strongly influences heme composition and rate and directionality of electron transfer in *Paracoccus denitrificans* cytochrome *c* oxidase. *J Biol Chem* 274: 37974–37981, 1999.
114. Karlsson B, Aasa R, Vanngård T, and Malmström BG. An EPR-detectable intermediate in the cytochrome oxidase-dioxygen reaction. *FEBS Lett* 131: 186–188, 1981.
115. Karlsson B and Andreasson LE. The identity of a new copper(II) electron paramagnetic resonance signal in cytochrome *c* oxidase. *Biochim Biophys Acta* 635: 73–80, 1981.
116. Karpefors M, Ädelroth P, Namslauer A, Zhen Y, and Brzezinski P. Formation of the "peroxy" intermediate in cytochrome *c* oxidase is associated with internal proton/hydrogen transfer. *Biochemistry* 39: 14664–14669, 2000.
117. Keilin D. On cytochrome, a respiratory pigment common to animals, yeast, and higher plants. *Proc R Soc Lond B Biol Sci* 98: 312–339, 1925.
118. Keilin D. Influence of carbon monoxide and light on indophenol oxidase of yeast cells. *Nature* 119: 670–671, 1927.
119. Kelly M, Lappalainen P, Talbo G, Haltia T, van der OJ, and Saraste M. Two cysteines, two histidines, and one methionine are ligands of a binuclear purple copper center. *J Biol Chem* 268: 16781–16787, 1993.
120. Kelly MJ, Poole RK, Yates MG, and Kennedy C. Cloning and mutagenesis of genes encoding the cytochrome *bd* terminal oxidase complex in *Azotobacter vinelandii*: mutants deficient in the cytochrome *d* complex are unable to fix nitrogen in air. *J Bacteriol* 172: 6010–6019, 1990.

121. Kirichenko A, Vygodina T, Mkrtchyan HM, and Konstantinov A. Specific cation binding site in mammalian cytochrome oxidase. *FEBS Lett* 423: 329–333, 1998.
122. Kobayashi K, Une H, and Hayashi K. Electron transfer process in cytochrome oxidase after pulse radiolysis. *J Biol Chem* 264: 7976–7980, 1989.
123. Konstantinov AA, Siletsky S, Mitchell D, Kaulen A, and Gennis RB. The roles of the two proton input channels in cytochrome *c* oxidase from *Rhodobacter sphaeroides* probed by the effects of site-directed mutations on time-resolved electrogenic intraprotein proton transfer. *Proc Natl Acad Sci U S A* 94: 9085–9090, 1997.
124. Krab K and Wikström M. Proton-translocating cytochrome *c* oxidase in artificial phospholipid vesicles. *Biochim Biophys Acta* 504: 200–214, 1978.
125. Kroneck PM, Antholine WE, Kastrau DH, Buse G, Steffens GC, and Zumft WG. Multifrequency EPR evidence for a bimetallic center at the Cu_A site in cytochrome *c* oxidase. *FEBS Lett* 268: 274–276, 1990.
126. LaMarche AE, Abate MI, Chan SH, and Trumpower BL. Isolation and characterization of *COX12*, the nuclear gene for a previously unrecognized subunit of *Saccharomyces cerevisiae* cytochrome *c* oxidase. *J Biol Chem* 267: 22473–22480, 1992.
127. Lanyi JK. X-ray diffraction of bacteriorhodopsin photocycle intermediates. *Mol Membr Biol* 21: 143–150, 2004.
128. Lappalainen P, Aasa R, Malmström BG, and Saraste M. Soluble Cu_A-binding domain from the *Paracoccus* cytochrome *c* oxidase. *J Biol Chem* 268: 26416–26421, 1993.
129. Larsen RW, Pan LP, Musser SM, Li ZY, and Chan SI. Could Cu_B be the site of redox linkage in cytochrome *c* oxidase? *Proc Natl Acad Sci U S A* 89: 723–727, 1992.
130. Lee A, Kirichenko A, Vygodina T, Siletsky SA, Das TK, Rousseau DL, Gennis R, and Konstantinov AA. Ca^{2+}-binding site in *Rhodobacter sphaeroides* cytochrome *c* oxidase. *Biochemistry* 41: 8886–8898, 2002.
131. Lee HM, Das TK, Rousseau DL, Mills D, Ferguson-Miller S, and Gennis RB. Mutations in the putative H-channel in the cytochrome *c* oxidase from *Rhodobacter sphaeroides* show that this channel is not important for proton conduction but reveal modulation of the properties of heme *a*. *Biochemistry* 39: 2989–2996, 2000.
132. Lemberg R. Action of alkali on cytochrome oxidase. *Nature* 193: 373–000, 1962.
133. Liao GL, Palmer G. The reduced minus oxidized difference spectra of cytochromes *a* and a_3. *Biochim Biophys Acta* 1274: 109–111, 1996.
134. Ma J, Tsatsos PH, Zaslavsky D, Barquera B, Thomas JW, Katsonouri A, Puustinen A, Wikstrom M, Brzezinski P, Alben JO, and Gennis RB. Glutamate-89 in subunit II of cytochrome *bo3* from *Escherichia coli* is required for the function of the heme-copper oxidase. *Biochemistry* 38: 15150–15156, 1999.
135. Malmström BG and Aasa R. The nature of the Cu_A center in cytochrome *c* oxidase. *FEBS Lett* 325: 49–52, 1993.
136. Marcus RA and Sutin N. Electron transfers in chemistry and biology. *Biochim Biophys Acta* 811: 265–322, 1985.
137. McCauley KM, Vrtis JM, Dupont J, and van der Donk WA. Insights into the functional role of the tyrosine-histidine linkage in cytochrome *c* oxidase. *J Am Chem Soc* 122: 2403–2404, 2000.
138. Michel H. The mechanism of proton pumping by cytochrome *c* oxidase. *Proc Natl Acad Sci U S A* 95: 12819–12824, 1998.
139. Miller MJ and Gennis RB. The cytochrome *d* complex is a coupling site in the aerobic respiratory chain of *Escherichia coli*. *J Biol Chem* 260: 14003–14008, 1985.
140. Mitchell P. Coupling of phosphorylation to electron and hydrogen transfer by a chemi-osmotic type of mechanism. *Nature* 191: 144–148, 1961.
141. Mitchell P. Possible molecular mechanisms of the protonmotive function of cytochrome systems. *J Theor Biol* 62: 327–367, 1976.
142. Mitchell P. Possible protonmotive osmochemistry in cytochrome oxidase. *Ann N Y Acad Sci* 550: 185–198, 1988.
143. Mitchell R, Mitchell P, and Rich PR. The assignment of the 655 nm spectral band of cytochrome oxidase. *FEBS Lett* 280: 321–324, 1991.
144. Mitchell R and Rich PR. Proton uptake by cytochrome *c* oxidase on reduction and on ligand binding. *Biochim Biophys Acta* 1186: 19–26, 1994.
145. Moody AJ, Brandt U, and Rich PR. Single electron reduction of "slow" and "fast" cytochrome-*c* oxidase. *FEBS Lett* 293: 101–105, 1991.
146. Moody AJ, Cooper CE, and Rich PR. Characterisation of "fast" and "slow" forms of bovine heart cytochrome-*c* oxidase. *Biochim Biophys Acta* 1059: 189–207, 1991.
147. Moody AJ and Rich PR. The effect of pH on redox titrations of haem *a* in cyanide-liganded cytochrome-*c* oxidase: experimental and modelling studies. *Biochim Biophys Acta* 1015: 205–215, 1990.
148. Morgan JE, Li PM, Jang DJ, el Sayed MA, and Chan SI. Electron transfer between cytochrome *a* and copper A in cytochrome *c* oxidase: a perturbed equilibrium study. *Biochemistry* 28: 6975–6983, 1989.
149. Morgan JE, Verkhovsky MI, Palmer G, and Wikström M. Role of the P_R intermediate in the reaction of cytochrome *c* oxidase with O_2. *Biochemistry* 40: 6882–6892, 2001.
150. Morgan JE, Verkhovsky MI, and Wikström M. The histidine cycle: a new model for proton translocation in the respiratory heme-copper oxidases. *J Bioenerg Biomembr* 26: 599–608, 1994.
151. Morgan JE, Verkhovsky MI, and Wikström M. Observation and assignment of peroxy and ferryl intermediates in the reduction of dioxygen to water by cytochrome *c* oxidase. *Biochemistry* 35: 12235–12240, 1996.
152. Moser CC, Keske JM, Warncke K, Farid RS, and Dutton PL. Nature of biological electron transfer. *Nature* 355: 796–802, 1992.
153. Muramoto K, Hirata K, Shinzawa-Itoh K, Yoko-o S, Yamashita E, Aoyama H, Tsukihara T, and Yoshikawa S. A histidine residue acting as a controlling site for dioxygen reduction and proton pumping by cytochrome *c* oxidase. *Proc Natl Acad Sci U S A* 104: 7881–7886, 2007.
154. Nagle JF and Morowitz HJ. Molecular mechanisms for proton transport in membranes. *Proc Natl Acad Sci U S A* 75: 298–302, 1978.
155. Nilsson T. Photoinduced electron transfer from tris(2,2′-bipyridyl)ruthenium to cytochrome *c* oxidase. *Proc Natl Acad Sci U S A* 89: 6497–6501, 1992.
156. Ogura T, Takahashi S, Shinzawa-Itoh K, Yoshikawa S, and Kitagawa T. Observation of the $Fe^{4+} = O$ stretching Raman band for cytochrome oxidase compound B at ambient temperature. *J Biol Chem* 265: 14721–14723, 1990.
157. Oliveberg M, Brzezinski P, and Malmström BG. The effect of pH and temperature on the reaction of fully reduced and mixed-valence cytochrome *c* oxidase with dioxygen. *Biochim Biophys Acta* 977: 322–328, 1989.
158. Oliveberg M, Hallen S, and Nilsson T. Uptake and release of protons during the reaction between cytochrome *c* oxidase and molecular oxygen: a flow-flash investigation. *Biochemistry* 30: 436–440, 1991.
159. Oliveberg M, Malmström BG. Internal electron transfer in cytochrome *c* oxidase: evidence for a rapid equilibrium between cytochrome *a* and the bimetallic site. *Biochemistry* 30: 7053–7057, 1991.
160. Oliveberg M, Malmström BG. Reaction of dioxygen with cytochrome *c* oxidase reduced to different degrees: indications of a transient dioxygen complex with copper-B. *Biochemistry* 31: 3560–3563, 1992.
161. Orii Y. Intermediates in the reaction of reduced cytochrome oxidase with dioxygen. *Ann N Y Acad Sci* 550: 105–117, 1988.
162. Ostermeier C, Harrenga A, Ermler U, and Michel H. Structure at 2.7 Å resolution of the *Paracoccus denitrificans* two-subunit cytochrome *c* oxidase complexed with an antibody FV fragment. *Proc Natl Acad Sci U S A* 94: 10547–10553, 1997.
163. Page CC, Moser CC, Chen X, and Dutton PL. Natural engineering principles of electron tunnelling in biological oxidation-reduction. *Nature* 402: 47–52, 1999.
164. Papa S, Capitanio N, and Villani G. A cooperative model for protonmotive heme-copper oxidases: the role of heme *a* in the proton pump of cytochrome *c* oxidase. *FEBS Lett* 439: 1–8, 1998.

165. Pelletier H and Kraut J. Crystal structure of a complex between electron-transfer partners, cytochrome *c* peroxidase and cytochrome *c*. *Science* 258: 1748–1755, 1992.
166. Pezeshk A, Torres J, Wilson MT, and Symons MC. The EPR spectrum for Cu_B in cytochrome *c* oxidase. *J Inorg Biochem* 83: 115–119, 2001.
167. Pfitzner U, Kirichenko A, Konstantinov AA, Mertens M, Wittershagen A, Kolbesen BO, Steffens GC, Harrenga A, Michel H, and Ludwig B. Mutations in the Ca^{2+} binding site of the *Paracoccus denitrificans* cytochrome *c* oxidase. *FEBS Lett* 456: 365–369, 1999.
168. Pfitzner U, Odenwald A, Ostermann T, Weingard L, Ludwig B, and Richter OM. Cytochrome *c* oxidase (heme aa_3) from *Paracoccus denitrificans*: analysis of mutations in putative proton channels of subunit I. *J Bioenerg Biomembr* 30: 89–97, 1998.
169. Pilet E, Jasaitis A, Liebl U, and Vos MH. Electron transfer between hemes in mammalian cytochrome *c* oxidase. *Proc Natl Acad Sci U S A* 101: 16198–16203, 2004.
170. Poole RK. Bacterial cytochrome oxidases: a structurally and functionally diverse group of electron-transfer proteins. *Biochim Biophys Acta* 726: 205–243, 1983.
171. Popovic DM and Stuchebrukhov AA. Proton pumping mechanism and catalytic cycle of cytochrome *c* oxidase: coulomb pump model with kinetic gating. *FEBS Lett* 566: 126–130, 2004.
172. Proshlyakov DA, Pressler MA, and Babcock GT. Dioxygen activation and bond cleavage by mixed-valence cytochrome *c* oxidase. *Proc Natl Acad Sci U S A* 95: 8020–8025, 1998.
173. Proshlyakov DA, Pressler MA, DeMaso C, Leykam JF, DeWitt DL, and Babcock GT. Oxygen activation and reduction in respiration: involvement of redox-active tyrosine 244. *Science* 290: 1588–1591, 2000.
174. Puustinen A, Finel M, Haltia T, Gennis RB, and Wikström M. Properties of the two terminal oxidases of *Escherichia coli*. *Biochemistry* 30: 3936–3942, 1991.
175. Puustinen A, Finel M, Virkki M, and Wikström M. Cytochrome *o* (*bo*) is a proton pump in P*aracoccus denitrificans* and *Escherichia coli*. *FEBS Lett* 249: 163–167, 1989.
176. Puustinen A and Wikström M. Proton exit from the heme-copper oxidase of *Escherichia coli*. *Proc Natl Acad Sci U S A* 96: 35–37, 1999.
177. Qin L, Hiser C, Mulichak A, Garavito RM, and Ferguson-Miller S. Identification of conserved lipid/detergent-binding sites in a high-resolution structure of the membrane protein cytochrome *c* oxidase. *Proc Natl Acad Sci U S A* 103: 16117–16122, 2006.
178. Raha S and Robinson BH. Mitochondria, oxygen free radicals, disease and ageing. *Trends Biochem Sci* 25: 502–508, 2000.
179. Raitio M, Jalli T, and Saraste M. Isolation and analysis of the genes for cytochrome *c* oxidase in *Paracoccus denitrificans*. *EMBO J* 6: 2825–2833, 1987.
180. Rauhamäki V, Baumann M, Soliymani R, Puustinen A, and Wikström M. Identification of a histidine-tyrosine cross-link in the active site of the cbb_3-type cytochrome *c* oxidase from *Rhodobacter sphaeroides*. *Proc Natl Acad Sci U S A* 103: 16135–16140, 2006.
181. Reinhammar B, Malkin R, Jensen P, Karlsson B, Andreasson LE, Aasa R, Vanngård T, and Malmström BG. A new copper(II) electron paramagnetic resonance signal in two laccases and in cytochrome *c* oxidase. *J Biol Chem* 255: 5000–5003, 1980.
182. Ribacka C, Verkhovsky MI, Belevich I, Bloch DA, Puustinen A, and Wikström M. An elementary reaction step of the proton pump is revealed by mutation of tryptophan-164 to phenylalanine in cytochrome *c* oxidase from *Paracoccus denitrificans*. *Biochemistry* 44: 16502–16512, 2005.
183. Rice CW and Hempfling WP. Oxygen-limited continuous culture and respiratory energy conservation in *Escherichia coli*. *J Bacteriol* 134: 115–124, 1978.
184. Rich PR, Jünemann S, and Meunier B. Protonmotive mechanism of heme-copper oxidases. *J Bioenerg Biomembr* 30: 131–138, 1998.
185. Rieder R, Bosshard HR. Comparison of the binding sites on cytochrome *c* for cytochrome *c* oxidase, cytochrome bc_1, and cytochrome c_1: differential acetylation of lysyl residues in free and complexed cytochrome *c*. *J Biol Chem* 255: 4732–4739, 1980.
186. Rigaud JL, Pitard B, and Levy D. Reconstitution of membrane proteins into liposomes: application to energy-transducing membrane proteins. *Biochim Biophys Acta* 1231: 223–246, 1995.
187. Riistama S, Hummer G, Puustinen A, Dyer RB, Woodruff WH, and Wikström M. Bound water in the proton translocation mechanism of the haem-copper oxidases. *FEBS Lett* 414: 275–280, 1997.
188. Riistama S, Laakkonen L, Wikström M, Verkhovsky MI, and Puustinen A. The calcium binding site in cytochrome aa_3 from *Paracoccus denitrificans*. *Biochemistry* 38: 10670–10677, 1999.
189. Riistama S, Puustinen A, Garcia-Horsman A, Iwata S, Michel H, and Wikström M. Channelling of dioxygen into the respiratory enzyme. *Biochim Biophys Acta* 1275: 1–4, 1996.
190. Riistama S, Puustinen A, Verkhovsky MI, Morgan JE, and Wikström M. Binding of O_2 and its reduction are both retarded by replacement of valine 279 by isoleucine in cytochrome *c* oxidase from *Paracoccus denitrificans*. *Biochemistry* 39: 6365–6372, 2000.
191. Riistama S, Verkhovsky MI, Laakkonen L, Wikström M, and Puustinen A. Interaction between the formyl group of heme *a* and arginine 54 in cytochrome aa_3 from *Paracoccus denitrificans*. *Biochim Biophys Acta* 1456: 1–4, 2000.
192. Rousseau DL, Ching Y, and Wang J. Proton translocation in cytochrome *c* oxidase: redox linkage through proximal ligand exchange on cytochrome a_3. *J Bioenerg Biomembr* 25: 165–176, 1993.
193. Ruitenberg M, Kannt A, Bamberg E, Fendler K, and Michel H. Reduction of cytochrome *c* oxidase by a second electron leads to proton translocation. *Nature* 417: 99–102, 2002.
194. Ruitenberg M, Kannt A, Bamberg E, Ludwig B, Michel H, and Fendler K. Single-electron reduction of the oxidized state is coupled to proton uptake via the K pathway in *Paracoccus denitrificans* cytochrome *c* oxidase. *Proc Natl Acad Sci U S A* 97: 4632–4636, 2000.
195. Saiki K, Mogi T, Ogura K, and Anraku Y. *In vitro* heme O synthesis by the *cyoE* gene product from *Escherichia coli*. *J Biol Chem* 268: 26041–26044, 1993.
196. Salomonsson L, Lee A, Gennis RB, and Brzezinski P. A single-amino-acid lid renders a gas-tight compartment within a membrane-bound transporter. *Proc Natl Acad Sci U S A* 101: 11617–11621, 2004.
197. Saraste M. Structural features of cytochrome oxidase. *Q Rev Biophys* 23: 331–366, 1990.
198. Saraste M. Oxidative phosphorylation at the *fin de siecle*. *Science* 283: 1488–1493, 1999.
199. Schmidt B, McCracken J, and Ferguson-Miller S. A discrete water exit pathway in the membrane protein cytochrome *c* oxidase. *Proc Natl Acad Sci U S A* 100: 15539–15542, 2003.
200. Seelig A, Ludwig B, Seelig J, and Schatz G. Copper and manganese electron spin resonance studies of cytochrome *c* oxidase from *Paracoccus denitrificans*. *Biochim Biophys Acta* 636: 162–167, 1981.
201. Semenza GL. Oxygen-dependent regulation of mitochondrial respiration by hypoxia-inducible factor 1. *Biochem J* 405: 1–9, 2007.
202. Shapleigh JP and Gennis RB. Cloning, sequencing and deletion from the chromosome of the gene encoding subunit I of the aa_3-type cytochrome *c* oxidase of *Rhodobacter sphaeroides*. *Mol Microbiol* 6: 635–642, 1992.
203. Shapleigh JP, Hosler JP, Tecklenburg MM, Kim Y, Babcock GT, Gennis RB, and Ferguson-Miller S. Definition of the catalytic site of cytochrome *c* oxidase: specific ligands of heme *a* and the heme a_3-Cu_B center. *Proc Natl Acad Sci U S A* 89: 4786–4790, 1992.
204. Shaw RW, Hansen RE, and Beinert H. Responses of the a_3 component of cytochrome *c* oxidase to substrate and ligand addition. *Biochim Biophys Acta* 504: 187–199, 1978.
205. Shimokata K, Katayama Y, Murayama H, Suematsu M, Tsukihara T, Muramoto K, Aoyama H, Yoshikawa S, and Shimada H. The proton pumping pathway of bovine heart cytochrome *c* oxidase. *Proc Natl Acad Sci U S A* 104: 4200–4205, 2007.
206. Siegbahn PEM, Blomberg MRA, and Blomberg ML. Theoretical study of the energetics of proton pumping and oxygen reduction in cytochrome oxidase. *J Phys Chem B* 107: 10946–10955, 2003.

207. Siletsky SA, Pawate AS, Weiss K, Gennis RB, and Konstantinov AA. Transmembrane charge separation during the ferryl-oxo → oxidized transition in a nonpumping mutant of cytochrome *c* oxidase. *J Biol Chem* 279: 52558–52565, 2004.
208. Slater EC. Keilin, cytochrome, and the respiratory chain. *J Biol Chem* 278: 16455–16461, 2003.
209. Smirnova IA, Ädelroth P, Gennis RB, and Brzezinski P. Aspartate-132 in cytochrome *c* oxidase from *Rhodobacter sphaeroides* is involved in a two-step proton transfer during oxo-ferryl formation. *Biochemistry* 38: 6826–6833, 1999.
210. Solioz M, Carafoli E, and Ludwig B. The cytochrome *c* oxidase of *Paracoccus denitrificans* pumps protons in a reconstituted system. *J Biol Chem* 257: 1579–1582, 1982.
211. Soulimane T, Buse G, Bourenkov GP, Bartunik HD, Huber R, and Than ME. Structure and mechanism of the aberrant ba_3-cytochrome *c* oxidase from *Thermus thermophilus*. *EMBO J* 19: 1766–1776, 2000.
212. Steinrucke P, Steffens GC, Panskus G, Buse G, and Ludwig B. Subunit II of cytochrome *c* oxidase from *Paracoccus denitrificans*. DNA sequence, gene expression and the protein. *Eur J Biochem* 167: 431–439, 1987.
213. Stock D, Gibbons C, Arechaga I, Leslie AG, and Walker JE. The rotary mechanism of ATP synthase. *Curr Opin Struct Biol* 10: 672–679, 2000.
214. Sucheta A, Szundi I, and Einarsdottir O. Intermediates in the reaction of fully reduced cytochrome *c* oxidase with dioxygen. *Biochemistry* 37: 17905–17914, 1998.
215. Svensson-Ek M, Abramson J, Larsson G, Tornroth S, Brzezinski P, and Iwata S. The X-ray crystal structures of wild-type and EQ(I-286) mutant cytochrome *c* oxidases from *Rhodobacter sphaeroides*. *J Mol Biol* 321: 329–339, 2002.
216. Svensson-Ek M, Thomas JW, Gennis RB, Nilsson T, and Brzezinski P. Kinetics of electron and proton transfer during the reaction of wild type and helix VI mutants of cytochrome bo_3 with oxygen. *Biochemistry* 35: 13673–13680, 1996.
217. Thomas JW, Calhoun MW, Lemieux LJ, Puustinen A, Wikström M, Alben JO, and Gennis RB. Site-directed mutagenesis of residues within helix VI in subunit I of the cytochrome bo_3 ubiquinol oxidase from *Escherichia coli* suggests that tyrosine 288 may be a Cu_B ligand. *Biochemistry* 33: 13013–13021, 1994.
218. Thomas JW, Lemieux LJ, Alben JO, and Gennis RB. Site-directed mutagenesis of highly conserved residues in helix VIII of subunit I of the cytochrome *bo* ubiquinol oxidase from *Escherichia coli*: an amphipathic transmembrane helix that may be important in conveying protons to the binuclear center. *Biochemistry* 32: 11173–11180, 1993.
219. Thomas JW, Puustinen A, Alben JO, Gennis RB, and Wikström M. Substitution of asparagine for aspartate-135 in subunit I of the cytochrome *bo* ubiquinol oxidase of *Escherichia coli* eliminates proton-pumping activity. *Biochemistry* 32: 10923–10928, 1993.
220. Tsukihara T, Aoyama H, Yamashita E, Tomizaki T, Yamaguchi H, Shinzawa-Itoh K, Nakashima R, Yaono R, and Yoshikawa S. Structures of metal sites of oxidized bovine heart cytochrome *c* oxidase at 2.8 Å. *Science* 269: 1069–1074, 1995.
221. Tsukihara T, Aoyama H, Yamashita E, Tomizaki T, Yamaguchi H, Shinzawa-Itoh K, Nakashima R, Yaono R, and Yoshikawa S. The whole structure of the 13-subunit oxidized cytochrome *c* oxidase at 2.8 Å. *Science* 272: 1136–1144, 1996.
222. Tsukihara T, Shimokata K, Katayama Y, Shimada H, Muramoto K, Aoyama H, Mochizuki M, Shinzawa-Itoh K, Yamashita E, Yao M, Ishimura Y, and Yoshikawa S. The low-spin heme of cytochrome *c* oxidase as the driving element of the proton-pumping process. *Proc Natl Acad Sci USA* 100: 15304–15309, 2003.
223. Turrens JF, Alexandre A, and Lehninger AL. Ubisemiquinone is the electron donor for superoxide formation by complex III of heart mitochondria. *Arch Biochem Biophys* 237: 408–414, 1985.
224. Turrens JF and Boveris A. Generation of superoxide anion by the NADH dehydrogenase of bovine heart mitochondria. *Biochem J* 191: 421–427, 1980.
225. Tweedle MF and Wilson LJ. Electronic state of heme in cytochrome oxidase III: the magnetic susceptibility of beef heart cytochrome oxidase and some of its derivatives from 7–200 K: direct evidence for an antiferromagnetically coupled Fe (III)/Cu (II) pair. *J Biol Chem* 253: 8065–8071, 1978.
226. van der OJ, Lappalainen P, Musacchio A, Warne A, Lemieux L, Rumbley J, Gennis RB, Aasa R, Pascher T, Malmström BG, and Saraste M. Restoration of a lost metal-binding site: construction of two different copper sites into a subunit of the *E. coli* cytochrome *o* quinol oxidase complex. *EMBO J* 11: 3209–3217, 1992.
227. Van Gelder BF and Beinert H. Studies of the heme components of cytochrome *c* oxidase by EPR spectroscopy. *Biochim Biophys Acta* 189: 1–24, 1969.
228. Vanneste WH. The stoichiometry and absorption spectra of components *a* and a_3 in cytochrome *c* oxidase. *Biochemistry* 5: 838–848, 1966.
229. Varotsis C and Babcock GT. Appearance of the $\nu(Fe^{IV} = O)$ vibration from a ferryl-oxo intermediate in the cytochrome oxidase/dioxygen reaction. *Biochemistry* 29: 7357–7362, 1990.
230. Varotsis C, Woodruff WH, and Babcock GT. Time-resolved Raman detection of upsilon(Fe-O) in an early intermediate in the reduction of O_2 by cytochrome oxidase. *J Am Chem Soc* 111: 6439–6440, 1989.
231. Varotsis C, Zhang Y, Appelman EH, and Babcock GT. Resolution of the reaction sequence during the reduction of O_2 by cytochrome oxidase. *Proc Natl Acad Sci U S A* 90: 237–241, 1993.
232. Verkhovskaya M, Verkhovsky M, and Wikström M. pH dependence of proton translocation by *Escherichia coli*. *J Biol Chem* 267: 14559–14562, 1992.
233. Verkhovskaya ML, Garcia-Horsman A, Puustinen A, Rigaud JL, Morgan JE, Verkhovsky MI, and Wikström M. Glutamic acid 286 in subunit I of cytochrome bo_3 is involved in proton translocation. *Proc Natl Acad Sci U S A* 94: 10128–10131, 1997.
234. Verkhovsky MI, Belevich I, Bloch DA, and Wikström M. Elementary steps of proton translocation in the catalytic cycle of cytochrome oxidase. *Biochim Biophys Acta* 1757: 401–407, 2006.
235. Verkhovsky MI, Jasaitis A, Verkhovskaya ML, Morgan JE, and Wikström M. Proton translocation by cytochrome *c* oxidase. *Nature* 400: 480–483, 1999.
236. Verkhovsky MI, Jasaitis A, and Wikström M. Ultrafast haemhaem electron transfer in cytochrome *c* oxidase. *Biochim Biophys Acta* 1506: 143–146, 2001.
237. Verkhovsky MI, Morgan JE, Puustein A, and Wikström M. Kinetic trapping of oxygen in cell respiration. *Nature* 380: 268–270, 1996.
238. Verkhovsky MI, Morgan JE, Puustinen A, and Wikström M. The "ferrous-oxy" intermediate in the reaction of dioxygen with fully reduced cytochromes aa_3 and bo_3. *Biochemistry* 35: 16241–16246, 1996.
239. Verkhovsky MI, Morgan JE, Verkhovskaya ML, and Wikström M. Translocation of electrical charge during a single turnover of cytochrome *c* oxidase. *Biochim Biophys Acta* 1318: 6–10, 1997.
240. Verkhovsky MI, Morgan JE, and Wikström M. Intramolecular electron transfer in cytochrome *c* oxidase: a cascade of equilibria. *Biochemistry* 31: 11860–11863, 1992.
241. Verkhovsky MI, Morgan JE, and Wikström M. Oxygen binding and activation: early steps in the reaction of oxygen with cytochrome *c* oxidase. *Biochemistry* 33: 3079–3086, 1994.
242. Verkhovsky MI, Morgan JE, and Wikström M. Control of electron delivery to the oxygen reduction site of cytochrome *c* oxidase: a role for protons. *Biochemistry* 34: 7483–7491, 1995.
243. Verkhovsky MI, Morgan JE, and Wikström M. Redox transitions between oxygen intermediates in cytochrome-*c* oxidase. *Proc Natl Acad Sci U S A* 93: 12235–12239, 1996.
244. Verkhovsky MI, Tuukkanen A, Backgren C, Puustinen A, and Wikström M. Charge translocation coupled to electron injection into oxidized cytochrome *c* oxidase from *Paracoccus denitrificans*. *Biochemistry* 40: 7077–7083, 2001.
245. Vygodina T and Konstantinov A. Effect of pH on the spectrum of cytochrome *c* oxidase hydrogen peroxide complex. *Biochim Biophys Acta* 973: 390–398, 1989.
246. Vygodina TV and Konstantinov AA. H_2O_2-induced conversion of cytochrome *c* oxidase peroxy complex to oxoferryl state. *Ann N Y Acad Sci* 550: 124–138, 1988.

247. Wikström M. Energy-dependent reversal of the cytochrome oxidase reaction. *Proc Natl Acad Sci U S A* 78: 4051–4054, 1981.
248. Wikström M. Two protons are pumped from the mitochondrial matrix per electron transferred between NADH and ubiquinone. *FEBS Lett* 169: 300–304, 1984.
249. Wikström M. Identification of the electron transfers in cytochrome oxidase that are coupled to proton-pumping. *Nature* 338: 776–778, 1989.
250. Wikström M, Jasaitis A, Backgren C, Puustinen A, and Verkhovsky MI. The role of the D- and K-pathways of proton transfer in the function of the haem-copper oxidases. *Biochim Biophys Acta* 1459: 514–520, 2000.
251. Wikström M, Krab K, and Saraste M. *Cytochrome Oxidase: A Synthesis.* London: Academic Press, 1981, p. 198.
252. Wikström M and Morgan JE. The dioxygen cycle: spectral, kinetic, and thermodynamic characteristics of ferryl and peroxy intermediates observed by reversal of the cytochrome oxidase reaction. *J Biol Chem* 267: 10266–10273, 1992.
253. Wikström M, Saari H, Penttilä T, and Saraste M. In: *Membrane proteins: 11th FEBS Meeting, Symposium A4.* POxford: Pergamon,1977, pp. 85–94.
254. Wikström M, Verkhovsky MI, and Hummer G. Water-gated mechanism of proton translocation by cytochrome *c* oxidase. *Biochim Biophys Acta* 1604: 61–65, 2003.
255. Wikström MK. Proton pump coupled to cytochrome *c* oxidase in mitochondria. *Nature* 266: 271–273, 1977.
256. Wikström MK and Saari HT. The mechanism of energy conservation and transduction by mitochondrial cytochrome *c* oxidase. *Biochim Biophys Acta* 462: 347–361, 1977.
257. Wilson DF, Erecinska M, and Owen CS. Some properties of the redox components of cytochrome *c* oxidase and their interactions. *Arch Biochem Biophys* 175: 160–172, 1976.
258. Wilson DF and Nelson D. Coulometric and potentiometric evaluation of the redox components of cytochrome *c* oxidase *in situ*. *Biochim Biophys Acta* 680: 233–241, 1982.
259. Witt H and Ludwig B. Isolation, analysis, and deletion of the gene coding for subunit IV of cytochrome *c* oxidase in *Paracoccus denitrificans*. *J Biol Chem* 272: 5514–5517, 1997.
260. Witt H, Malatesta F, Nicoletti F, Brunori M, and Ludwig B. Tryptophan 121 of subunit II is the electron entry site to cytochrome *c* oxidase in *Paracoccus denitrificans:* involvement of a hydrophobic patch in the docking reaction. *J Biol Chem* 273: 5132–5136, 1998.
261. Woodruff WH, Einarsdottir O, Dyer RB, Bagley KA, Palmer G, Atherton SJ, Goldbeck RA, Dawes TD, and Kliger DS. Nature and functional implications of the cytochrome a_3 transients after photodissociation of CO-cytochrome oxidase. *Proc Natl Acad Sci U S A* 88: 2588–2592, 1991.
262. Wrigglesworth JM. Formation and reduction of a "peroxy" intermediate of cytochrome *c* oxidase by hydrogen peroxide. *Biochem J* 217: 715–719, 1984.
263. Yang WL, Iacono L, Tang WM, and Chin KV. Novel function of the regulatory subunit of protein kinase A: regulation of cytochrome *c* oxidase activity and cytochrome *c* release. *Biochemistry* 37: 14175–14180, 1998.
264. Yano T. The energy-transducing NADH: quinone oxidoreductase, complex I. *Mol Aspects Med* 23: 345–368, 2002.
265. Yoshikawa S, Shinzawa-Itoh K, Nakashima R, Yaono R, Yamashita E, Inoue N, Yao M, Fei MJ, Libeu CP, Mizushima T, Yamaguchi H, Tomizaki T, and Tsukihara T. Redox-coupled crystal structural changes in bovine heart cytochrome *c* oxidase. *Science* 280: 1723–1729, 1998.
266. Zaslavsky D, Kaulen AD, Smirnova IA, Vygodina T, and Konstantinov AA. Flash-induced membrane potential generation by cytochrome *c* oxidase. *FEBS Lett* 336: 389–393, 1993.
267. Zaslavsky D, Sadoski RC, Wang K, Durham B, Gennis RB, and Millett F. Single electron reduction of cytochrome *c* oxidase compound F: resolution of partial steps by transient spectroscopy. *Biochemistry* 37: 14910–14916, 1998.
268. Zhang DX and Gutterman DD. Mitochondrial reactive oxygen species-mediated signaling in endothelial cells. *Am J Physiol Heart Circ Physiol* 292: H2023–H2031, 2007.
269. Zhen Y, Hoganson CW, Babcock GT, and Ferguson-Miller S. Definition of the interaction domain for cytochrome *c* on cytochrome *c* oxidase, I: biochemical, spectral, and kinetic characterization of surface mutants in subunit ii of *Rhodobacter sphaeroides* cytochrome aa_3. *J Biol Chem* 274: 38032–38041, 1999.
270. Zheng X, Medvedev DM, Swanson J, and Stuchebrukhov AA. Computer simulation of water in cytochrome *c* oxidase. *Biochim Biophys Acta* 1557: 99–107, 2003.
271. Zickermann V, Verkhovsky M, Morgan J, Wikström M, Anemuller S, Bill E, Steffens GC, and Ludwig B. Perturbation of the Cu_A site in cytochrome-*c* oxidase of *Paracoccus denitrificans* by replacement of Met227 with isoleucine. *Eur J Biochem* 234: 686–693, 1995.

Address reprint requests to:
Michael I. Verkhovsky
Helsinki Bioenergetics Group
Program for Structural Biology and Biophysics
Institute of Biotechnology
PB 65 (Viikinkaari 1)
00014 University of Helsinki
Helsinki, Finland

E-mail: Michael.Verkhovsky@helsinki.fi

Date of first submission to ARS Central, April 17, 2007; date of acceptance, August 1, 2007.

This article has been cited by:

1. Hendrik A. Heering. 2012. Analysis of protein film voltammograms as Michaelis–Menten saturation curves yield the electron cooperativity number for deconvolution. *Bioelectrochemistry* **87**, 58-64. [CrossRef]
2. M. D. Mamedov, V. N. Kurashov, I. O. Petrova, A. Yu. Semenov. 2012. Transmembrane electric potential difference in the protein-pigment complex of photosystem 2. *Biochemistry (Moscow)* **77**:9, 947-955. [CrossRef]
3. Marina Verkhovskaya, Dmitry A. Bloch. 2012. Energy-converting respiratory Complex I: On the way to the molecular mechanism of the proton pump. *The International Journal of Biochemistry & Cell Biology* . [CrossRef]
4. Sergey A. Siletsky, Ilya Belevich, Tewfik Soulimane, Michael I. Verkhovsky, Mårten Wikström. 2012. The fifth electron in the fully reduced caa3 from Thermus thermophilus is competent in proton pumping. *Biochimica et Biophysica Acta (BBA) - Bioenergetics* . [CrossRef]
5. T. V. Vygodina, A. V. Dyuba, A. A. Konstantinov. 2012. Effect of calcium ions on electron transfer between hemes a and a 3 in cytochrome c oxidase. *Biochemistry (Moscow)* **77**:8, 901-909. [CrossRef]
6. Johannes B. M. Klok, Pim L. F. van den Bosch, Cees J. N. Buisman, Alfons J. M. Stams, Karel J. Keesman, Albert J. H. Janssen. 2012. Pathways of Sulfide Oxidation by Haloalkaliphilic Bacteria in Limited-Oxygen Gas Lift Bioreactors. *Environmental Science & Technology* **46**:14, 7581-7586. [CrossRef]
7. Christoph von Ballmoos, Peter Lachmann, Robert B. Gennis, Pia Ädelroth, Peter Brzezinski. 2012. Timing of Electron and Proton Transfer in the ba 3 Cytochrome c Oxidase from Thermus thermophilus. *Biochemistry* **51**:22, 4507-4517. [CrossRef]
8. H.-Y. Chang, S. K. Choi, A. S. Vakkasoglu, Y. Chen, J. Hemp, J. A. Fee, R. B. Gennis. 2012. Exploring the proton pump and exit pathway for pumped protons in cytochrome ba3 from Thermus thermophilus. *Proceedings of the National Academy of Sciences* . [CrossRef]
9. Michelle A. Yu, Tsuyoshi Egawa, Kyoko Shinzawa-Itoh, Shinya Yoshikawa, Victor Guallar, Syun-Ru Yeh, Denis L. Rousseau, Gary J. Gerfen. 2012. Two Tyrosyl Radicals Stabilize High Oxidation States in Cytochrome c Oxidase for Efficient Energy Conservation and Proton Translocation. *Journal of the American Chemical Society* 120306073545005. [CrossRef]
10. Linda Näsvik Öjemyr, Christoph von Ballmoos, Robert B. Gennis, Stephen G. Sligar, Peter Brzezinski. 2012. Reconstitution of respiratory oxidases in membrane nanodiscs for investigation of proton-coupled electron transfer. *FEBS Letters* **586**:5, 640-645. [CrossRef]
11. Alexander A. Konstantinov. 2012. Cytochrome c oxidase: Intermediates of the catalytic cycle and their energy-coupled interconversion. *FEBS Letters* **586**:5, 630-639. [CrossRef]
12. Lidia Gebicka, Katarzyna Stawowska. 2012. Spectrophotometric studies of the reaction of quercetin with peroxynitrite at different pH. *Central European Journal of Chemistry* **10**:1, 187-193. [CrossRef]
13. Linda Näsvik Öjemyr, Christoph von Ballmoos, Kristina Faxén, Emelie Svahn, Peter Brzezinski. 2012. The Membrane Modulates Internal Proton Transfer in Cytochrome c Oxidase. *Biochemistry* 120201121641004. [CrossRef]
14. Christoph von Ballmoos, Pia Ädelroth, Robert B. Gennis, Peter Brzezinski. 2011. Proton transfer in ba3 cytochrome c oxidase from Thermus thermophilus. *Biochimica et Biophysica Acta (BBA) - Bioenergetics* . [CrossRef]
15. Vitaliy B. Borisov, Robert B. Gennis, James Hemp, Michael I. Verkhovsky. 2011. The cytochrome bd respiratory oxygen reductases. *Biochimica et Biophysica Acta (BBA) - Bioenergetics* **1807**:11, 1398-1413. [CrossRef]
16. Mårten Wikström. 2011. Michael I. Verkhovsky (1953–2011). *Biochimica et Biophysica Acta (BBA) - Bioenergetics* . [CrossRef]
17. Marko Rintanen, Ilya Belevich, Michael I. Verkhovsky. 2011. Electrogenic events upon photolysis of CO from fully reduced cytochrome c oxidase. *Biochimica et Biophysica Acta (BBA) - Bioenergetics* . [CrossRef]
18. M. Trouillard, B. Meunier, F. Rappaport. 2011. PNAS Plus: Questioning the functional relevance of mitochondrial supercomplexes by time-resolved analysis of the respiratory chain. *Proceedings of the National Academy of Sciences* . [CrossRef]
19. Sergey A. Siletsky, Alexander A. Konstantinov. 2011. Cytochrome c oxidase: Charge translocation coupled to single-electron partial steps of the catalytic cycle. *Biochimica et Biophysica Acta (BBA) - Bioenergetics* . [CrossRef]
20. N. Kim, M.O. Ripple, R. Springett. 2011. Spectral components of the #-band of cytochrome oxidase. *Biochimica et Biophysica Acta (BBA) - Bioenergetics* **1807**:7, 779-787. [CrossRef]
21. C. von Ballmoos, R. B. Gennis, P. Adelroth, P. Brzezinski. 2011. Kinetic design of the respiratory oxidases. *Proceedings of the National Academy of Sciences* . [CrossRef]

22. Michelle A. Yu, Tsuyoshi Egawa, Kyoko Shinzawa-Itoh, Shinya Yoshikawa, Syun-Ru Yeh, Denis L. Rousseau, Gary J. Gerfen. 2011. Radical formation in cytochrome c oxidase. *Biochimica et Biophysica Acta (BBA) - Bioenergetics* . [CrossRef]
23. A Lemarie, S Grimm. 2011. Mitochondrial respiratory chain complexes: apoptosis sensors mutated in cancer?. *Oncogene* . [CrossRef]
24. Ann-Louise Johansson, Suman Chakrabarty, Catrine L. Berthold, Martin Högbom, Arieh Warshel, Peter Brzezinski. 2011. Proton-transport mechanisms in cytochrome c oxidase revealed by studies of kinetic isotope effects. *Biochimica et Biophysica Acta (BBA) - Bioenergetics* . [CrossRef]
25. Gianni Colotti, Andrea Ilari. 2011. Polyamine metabolism in Leishmania: from arginine to trypanothione. *Amino Acids* **40**:2, 269-285. [CrossRef]
26. Giuseppe Capitanio, Pietro Luca Martino, Nazzareno Capitanio, Sergio Papa. 2011. Redox Bohr effects and the role of heme a in the proton pump of bovine heart cytochrome c oxidase. *Biochimica et Biophysica Acta (BBA) - Bioenergetics* . [CrossRef]
27. Artem V. Dyuba, Alexander M. Arutyunyan, Tatiana V. Vygodina, Natalia V. Azarkina, Anastasia V. Kalinovich, Yuri A. Sharonov, Alexander A. Konstantinov. 2011. Circular dichroism spectra of cytochrome c oxidase. *Metallomics* **3**:4, 417. [CrossRef]
28. I. A. Bolshakov, T. V. Vygodina, R. Gennis, A. A. Karyakin, A. A. Konstantinov. 2010. Catalase Activity of Cytochrome c Oxidase Assayed with Hydrogen Peroxide-Sensitive Electrode Microsensor. *Biochemistry (Moscow)* **75**:11, 1352-1360. [CrossRef]
29. I. Belevich, E. Gorbikova, N. P. Belevich, V. Rauhamaki, M. Wikstrom, M. I. Verkhovsky. 2010. Initiation of the proton pump of cytochrome c oxidase. *Proceedings of the National Academy of Sciences* **107**:43, 18469-18474. [CrossRef]
30. I. O. Mazunin, N. V. Volodko, E. B. Starikovskaya, R. I. Sukernik. 2010. Mitochondrial genome and human mitochondrial diseases. *Molecular Biology* **44**:5, 665-681. [CrossRef]
31. Marc T. M. Koper, Hendrik A. HeeringComparison of Electrocatalysis and Bioelectrocatalysis of Hydrogen and Oxygen Redox Reactions 71-110. [CrossRef]
32. Aline C Pereira, Vania C Olivon, Ana Maria de Oliveira. 2010. An Apparent Paradox: Attenuation of Phenylephrine-mediated Calcium Mobilization and Hyperreactivity to Phenylephrine in Contralateral Carotid After Balloon Injury. *Journal of Cardiovascular Pharmacology* **56**:2, 162-170. [CrossRef]
33. Martin Trouillard, Brigitte Meunier, Fabrice Rappaport. 2010. Turning the mitochondrion into a chloroplast: the light-activation of the respiratory function in Saccharomyces cerevisiae allows its time-resolved analysis. *Biochimica et Biophysica Acta (BBA) - Bioenergetics* **1797**, 24. [CrossRef]
34. Giorgio Lenaz , Maria Luisa Genova . 2010. Structure and Organization of Mitochondrial Respiratory Complexes: A New Understanding of an Old Subject. *Antioxidants & Redox Signaling* **12**:8, 961-1008. [Abstract] [Full Text HTML] [Full Text PDF] [Full Text PDF with Links]
35. Kazuaki Yoshimune, Hajime Morimoto, Yu Hirano, Junshi Sakamoto, Hidetoshi Matsuyama, Isao Yumoto. 2010. The obligate alkaliphile Bacillus clarkii K24-1U retains extruded protons at the beginning of respiration. *Journal of Bioenergetics and Biomembranes* **42**:2, 111-116. [CrossRef]
36. Changyuan Lu, Xuan Zhao, Yi Lu, Denis L. Rousseau, Syun-Ru Yeh. 2010. Role of Copper Ion in Regulating Ligand Binding in a Myoglobin-Based Cytochrome c Oxidase Model. *Journal of the American Chemical Society* **132**:5, 1598-1605. [CrossRef]
37. D. M. Popovic, I. V. Leontyev, D. G. Beech, A. A. Stuchebrukhov. 2010. Similarity of cytochrome c oxidases in different organisms. *Proteins: Structure, Function, and Bioinformatics* n/a-n/a. [CrossRef]
38. Giorgio Lenaz, Maria Luisa Genova. 2009. Structural and functional organization of the mitochondrial respiratory chain: A dynamic super-assembly. *The International Journal of Biochemistry & Cell Biology* **41**:10, 1750-1772. [CrossRef]
39. M. S. Fernandes, M. M. Reddy, J. R. Gonneville, S. C. DeRoo, K. Podar, J. D. Griffin, D. M. Weinstock, M. Sattler. 2009. BCR-ABL promotes the frequency of mutagenic single-strand annealing DNA repair. *Blood* **114**:9, 1813-1819. [CrossRef]
40. Dmitry A. Bloch, Audrius Jasaitis, Michael I. Verkhovsky. 2009. Elevated Proton Leak of the Intermediate OH in Cytochrome c Oxidase. *Biophysical Journal* **96**:11, 4733-4742. [CrossRef]
41. Oliver-Matthias H. Richter, Bernd Ludwig. 2009. Electron transfer and energy transduction in the terminal part of the respiratory chain — Lessons from bacterial model systems. *Biochimica et Biophysica Acta (BBA) - Bioenergetics* **1787**:6, 626-634. [CrossRef]

42. Sergey A. Siletsky, Ilya Belevich, Mårten Wikström, Tewfik Soulimane, Michael I. Verkhovsky. 2009. Time-resolved OH#EH transition of the aberrant ba3 oxidase from Thermus thermophilus. *Biochimica et Biophysica Acta (BBA) - Bioenergetics* **1787**:3, 201-205. [CrossRef]
43. M. Bernroitner, M. Zamocky, P. G. Furtmuller, G. A. Peschek, C. Obinger. 2009. Occurrence, phylogeny, structure, and function of catalases and peroxidases in cyanobacteria. *Journal of Experimental Botany* **60**:2, 423-440. [CrossRef]
44. Dong Li, Mildred S. Yang, Tao Lin, Wei Zheng, Jianan Y. Qu. 2009. Study of cadmium-induced cytotoxicity using two-photon excitation endogenous fluorescence microscopy. *Journal of Biomedical Optics* **14**:5, 054028. [CrossRef]
45. Dong Li, Wei Zheng, Jianan Y. Qu. 2008. Time-resolved spectroscopic imaging reveals the fundamentals of cellular NADH fluorescence. *Optics Letters* **33**:20, 2365. [CrossRef]
46. Martyn A. Sharpe, Shelagh Ferguson-Miller. 2008. A chemically explicit model for the mechanism of proton pumping in heme–copper oxidases. *Journal of Bioenergetics and Biomembranes* **40**:5, 541-549. [CrossRef]
47. Freya A. Bundschuh, Klaus Hoffmeier, Bernd Ludwig. 2008. Two variants of the assembly factor Surf1 target specific terminal oxidases in Paracoccus denitrificans. *Biochimica et Biophysica Acta (BBA) - Bioenergetics* **1777**:10, 1336-1343. [CrossRef]
48. Flavia Fontanesi, Ileana C. Soto, Antoni Barrientos. 2008. Cytochrome c oxidase biogenesis: New levels of regulation. *IUBMB Life* **60**:9, 557-568. [CrossRef]
49. Irina A. Smirnova, Dmitry Zaslavsky, James A. Fee, Robert B. Gennis, Peter Brzezinski. 2008. Electron and proton transfer in the ba 3 oxidase from Thermus thermophilus. *Journal of Bioenergetics and Biomembranes* **40**:4, 281-287. [CrossRef]
50. Peter Greiner, Achim Hannappel, Carolin Werner, Bernd Ludwig. 2008. Biogenesis of cytochrome c oxidase — in vitro approaches to study cofactor insertion into a bacterial subunit I. *Biochimica et Biophysica Acta (BBA) - Bioenergetics* **1777**:7-8, 904-911. [CrossRef]
51. Suresh I.S. Rattan. 2008. Increased molecular damage and heterogeneity as the basis of aging. *Biological Chemistry* **389**:3, 267-272. [CrossRef]
52. Jaideep J. Pandit. 2008. Structure–Function Relationships: A Breath of Fresh Air – or Just More Hot Air – in Sleep Apnoea Research?. *Respiration* **76**:1, 16-18. [CrossRef]